A study of the effect of prior austenite grain size on the microstructure of Quenching and Partitioning steels with Phase-Field Modelling

Submitted by

Efstratios Koufis

In fulfilment of the requirements for the award of the degree of

MSc in Materials Science and Engineering

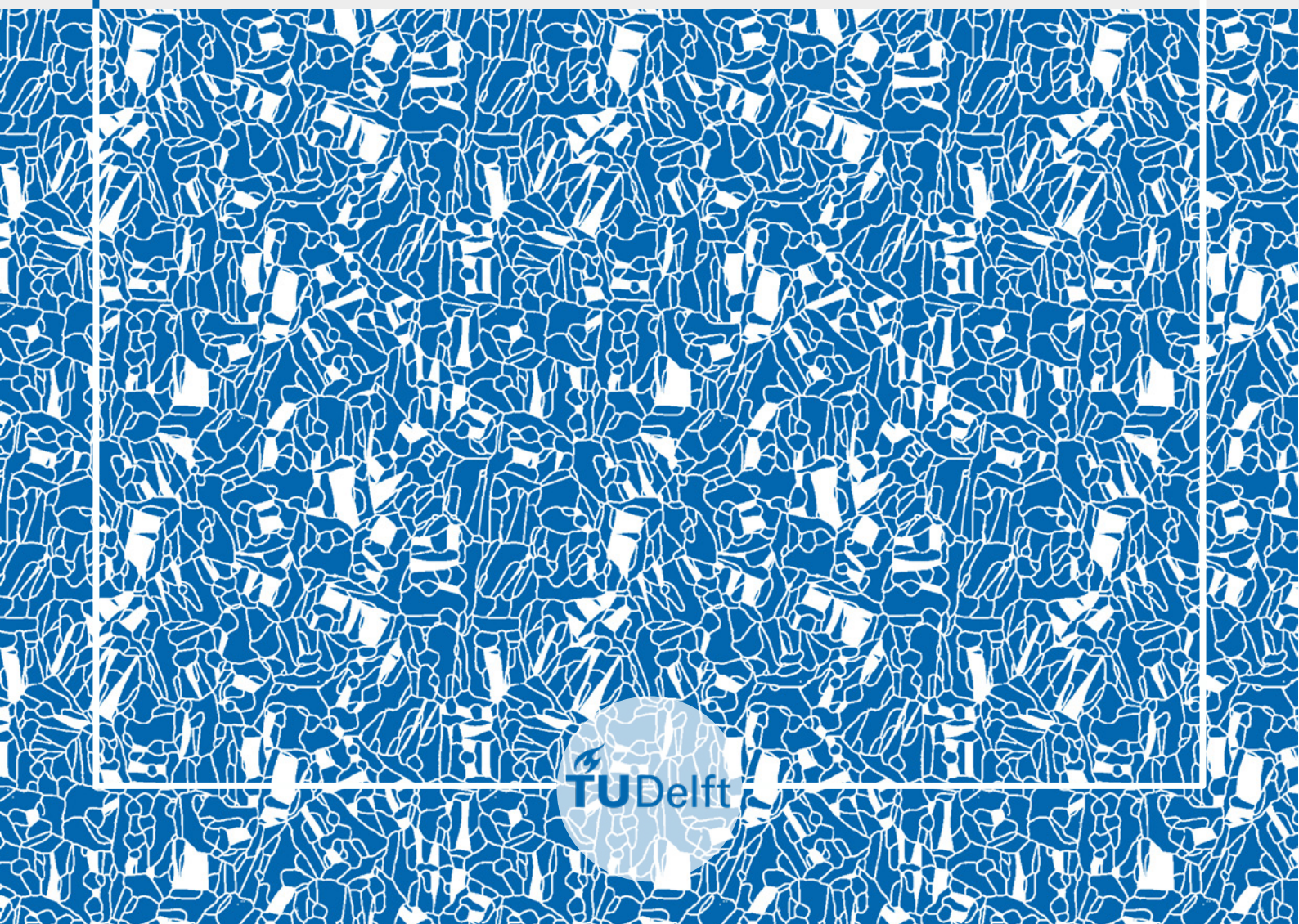

A study of the effect of prior austenite grain size on the microstructure of Quenching and Partitioning steels with Phase-Field Modelling

Thesis committee:

Prof. Dr. Maria J. Santofimia Navarro

Dr. Carola de Celada Casero

Dr. M.G. Mecozzi

Sudhindra Ayenampudi

Dr. Marcel H.F. Sluiter

to be defended publicly on Friday December 11, 2020 at 13:00.

An electronic version of this thesis is available at http://repository.tudelft.nl/.

Department of Materials Science & Engineering

Delft University of Technology

Delft, Netherlands

(December, 2020)

ACKNOWLEDGMENTS

Firstly, I would like to express my deep gratitude to Prof.dr. Maria J. Santofimia Navarro for giving me the opportunity to explore further the fascinating field of steel science. Her patient guidance and excellent supervision were key factors during the tough times of the COVID-19 pandemic.

I would also like to thank Dr. M.G. Mecozzi, Dr. Carola de Celada Casero and Ayenampudi Sudhindra. Without their help and their feedback, this work would not have been possible. The regular meetings helped me to proceed with my work and also kept reminding me to stay focused on my project during the pandemic. I felt that you were always willing to help me, and that was important to me.

I want to thank dr. Marcel H.F. Sluiter for accepting to be in the committee of my defence. Moreover, the courses in computational materials science, that he taught me, triggered me to work with phase-field modelling for my graduation project.

I also want to thank Drs. R.M. Huizenga for providing me with a licence for the software I used so that I could work remotely because of the current restrictions.

Special thanks go to Eleni Maria Koskeridou for designing the cover of my thesis.

I would also like to thank all my friends in the Netherlands for making this study period special. Special thanks also to my friends that were away physically, but they have always been supporting me.

Finally, I would like to thank my parents for their endless and unconditional support during my academic life; nothing would have been possible without them.

Efstratios Koufis

ABSTRACT

Quenching and partitioning (Q&P) is a novel processing route that can create microstructures that combine high strength, ductility and easy formability without the excess use of alloying elements by also keeping the production cost low. Therefore, this method is ideal to be applied to steels that are used in the automotive industry.

The material is initially annealed at a high temperature to form austenite. Then it is quenched to a temperature below the martensite start temperature to form a controlled fraction of martensite. Second annealing follows, at a lower temperature than the first one, that stabilises the austenitic phase at room temperature. It has been found that the austenite grain size at the end of the first annealing (prior austenite grain size) has a significant impact on the processing method, the final microstructure and consequently on the final properties of the material.

In this thesis, phase-field modelling was employed to investigate the role of prior austenite grain size on the quenching and partitioning process. Simulations of the processing were performed for three different prior austenite grain sizes (6, 25 and 67 μm). Microstructures consisting of about 10.5% austenite and 89.5% martensite were created by simulating the first quenching of the Q&P process. Then, the evolution of the microstructure and carbon distribution were investigated for partitioning at 400 $^{\circ}C$ for times up to 4000 s, and quenching to room temperature.

The results gave insights into the effect of the prior austenite grain size on the morphology of the microstructure and the kinetics of carbon during partitioning. It was found that a finer microstructure was derived with decreasing PAGS. Moreover, partitioning becomes more efficient because of the shorter distance that carbon has to diffuse, and the even spatial distribution of austenite.

Finally, wide grain size distributions of the austenite that is present during partitioning can lead to significant variations in the carbon content among the austenite grains of the final microstructure, especially for short partitioning times. This affects the efficiency of the partitioning process and has an impact on the mechanical stability of the austenite in the final microstructure and consequently on the TRIP phenomenon.

Contents

List of Figures

List of Tables

Chapter 1

Introduction

1.1 The three generations of advanced high strength steels

The development of high strength steels that meet the requirements set by the automotive industry is of great importance. Namely, high strength results in thinner sheets, smaller cross-sections of structural elements and consequently in lower weight and fuel consumption [1]. The low fuel consumption has a positive impact on the environment and also the transportation of people and goods becomes more affordable. However, it is discussed in the literature that under some circumstances, weight reduction can reduce the safety of a car and a trade-off between safety and fuel consumption exists [2]. So, it is also vital that the material that is used protects the passengers by absorbing the energy in case of a crash accident. Easy formability is also an important factor in the designing of new microstructures since the metal sheets have to be formed to the right shape.

Three generations of AHSS have been developed so far to satisfy the requirements mentioned above [1, 3].

- The first generation of AHSS consists of dual-phase steels (ferrite-martensite), complex-phase steels and transformation-induced plasticity steels (TRIP steels). The first generation showed better performance in terms of strength and ductility than conventional steels without a significant increase in the production cost.

- The second generation of AHSS consists of lightweight with induced plasticity (L-IP) steels, twin-induced plasticity (TWIP) steels and austenitic stainless steels along with other types of steel. In many of these steels, a specific fraction of austenite (about 0.10-0.20) needs to be present in the final microstructure at room temperature to give ductility to the material. However, to enhance austenite thermal stability, alloying elements such as Ni and Mn are used in high concentrations that increase the cost significantly.

- The third generation of AHSS is based on the development of steels with high

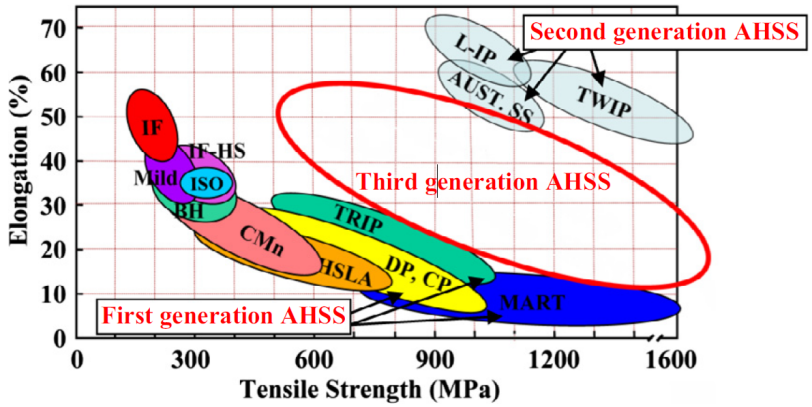

Figure 1.1: Elongation and tensile strength graph for different types of steels. The first three generations of AHSS are also shown in the figure [4].

strength and ductility but with low costs. The cost reduction is achieved by adding smaller concentrations of alloying elements and by applying new processing routes, also aiming to reduce the processing time. An example is the quenching and partitioning (Q&P) processing route that is discussed thoroughly in this report.

In figure 1.1 the tensile strength and the final elongation of the first two generations of AHSS and some conventional high strength steels are presented. Furthermore, the area where the third generation of AHSS lies on is marked.

1.2 The quenching and partitioning process

Q&P is a new processing method that can lead to microstructures containing stabilised austenite at room temperature without the need for excess alloying element usage. The thermal cycle of the process is presented in figure 1.2. The material initially is annealed at a temperature (T_γ) which is above the A_3 temperature where it undergoes full austenitisation. Then, the material is quenched rapidly to a temperature (T_Q) which is in between the martensitic transformation start temperature (M_S) and the martensitic transformation finish temperature (M_F) to introduce a controlled fraction of martensite in the microstructure. The resulting microstructure consists of a combination of martensite and austenite with martensite being the dominant phase. The final step is the partitioning step where the material is held at the T_Q or at a slightly increased temperature (T_P) for sufficient time to trigger the partitioning of carbon from martensite to austenite. Partitioning is the step that stabilises austenite thermally at room temperature. The chemical potential difference of carbon in austenite and martensite gives rise to this process. A final quenching to room

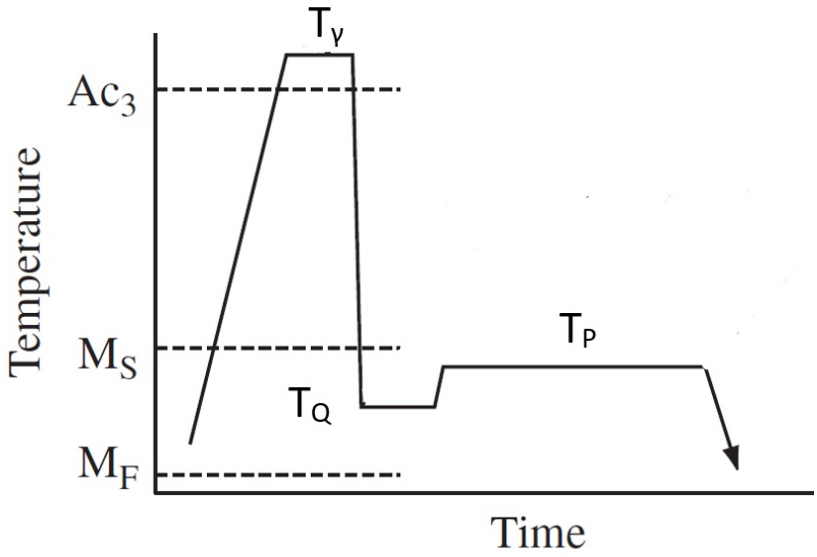

Figure 1.2: Thermal cycle of the quenching and partitioning process.

temperature ends the thermal treatment.

The final microstructure consists of martensite formed at the first quenching (M_1), retained austenite (RA), and often martensite formed at the final quench (M_2) resulting from the fraction of the austenite that could not be stabilised at room temperature [1]. Nevertheless, more complex microstructures can be created using the Q&P process. If the first annealing step is done at an intercritical temperature (between A_1 and A_3), the material does not transform fully to austenite and ferrite is present in the microstructure during the whole process. For the intercritical annealing case, the final microstructure consists of ferrite, M_1, RA and M_2 [5].

Considering the martensite morphology, it is known that it exhibits a characteristic hierarchical structure consisting of packets, blocks, sub-blocks and laths as it is depicted in figure 1.3 [6]. A packet consists of a group of parallel blocks and a block consists of sub-blocks of two different types. Finally, a sub-block consists of laths of the same Kurdjumov-Sachs (K-S) variant.

A characteristic of the blocks that belong to the same packet is that the laths of their sub-blocks share the same habit plane. Two different types of sub-blocks can exist in the same block, the difference between these two types is a misorientation of approximately 10 degrees between the laths of each type. Block and packet boundaries are considered to be high angle boundaries; the packet and the block size have an important impact on the mechanical strength of the material [7–9].

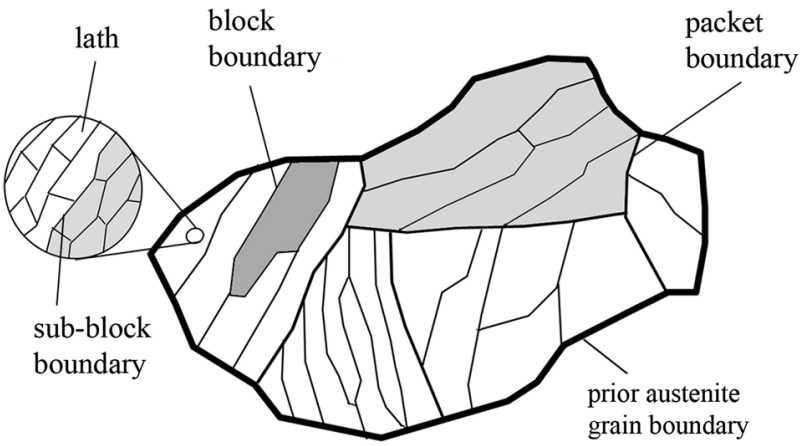

Figure 1.3: Representation of martensite morphology; lath, block, sub-block, packet and prior austenite grain boundaries are shown [6].

Retained austenite is usually present in Q&P microstructures either as film or block austenite [10, 11]. Film austenite is usually found between laths while blocks of austenite are found adjacent to prior austenite grain boundaries [12].

During the partitioning step of the Q&P route, processes that compete with carbon partitioning from martensite to austenite can occur, such as carbide precipitation or bainite formation. Both can change the final microstructure by affecting the phase composition or by consuming the carbon that is intended to partition to austenite and thus, making partitioning less efficient. Therefore, the chemical composition of the Q&P steels is selected aiming to stabilise austenite, to suppress carbide precipitation and to retard bainitic transformation when the material is held at the partitioning temperature [13].

Prior austenite grain size (PAGS) is of great importance for the Q&P process. PAGS is the size of the parent austenite grain after the austenitisation step and just before the first quenching, it can be determined experimentally, and there are different methods to control it. It is essential to control PAGS because it contributes to the production of refined microstructures. Some of the methods employed in steel processing and also control PAGS are listed below.

- PAGS can be controlled by changing the temperature and duration of the austenitisation process. Longer annealing times and higher temperatures increase PAGS [14].

- Application of thermomechanical processing methods such as hot-rolling while the material is held at the T_γ can refine the austenitic microstructure [11]. Also, cold rolling before the implementation of the Q&P process can reduce PAGS. [15].

- More complex thermal cycles, such as pre-quenching the material before applying Q&P (QQ&P) can be applied to create a finer microstructure by introducing more austenite nucleation sites before the actual Q&P process [10].

- Thermal cycling between T_γ and T_Q to the material before applying the Q&P process can reduce the PAGS effectively [6, 12].

Experiments often require support by simulation work since simulations can provide information that is difficult to be derived experimentally due to physical restrictions. This explains the application of phase-field modelling to study the stages of the Q&P process. Phenomena occurring during the Q&P process such as martensite nucleation and growth, and carbon redistribution during partitioning have been modelled adequately using this method and the results contributed to the better understanding of the Q&P process [16–18].

1.3 Phase field modelling in steel science research

Phase-field modelling (PFM) is used widely in microstructural evolution modelling. It has been used succesfully to simulate phenomena such as solidification, martensitic transformation, austenite reversion and the effect of PAGS on the martensitic transformation in a Fe-Ni alloy [18]. Furthermore, recrystallisation and grain growth has been modelled using PFM and also the evolution of the heat-affected zone that is formed during welding has drawn attention. In addition, displacive transformations such as the martensitic transformation have been simulated as it was a diffusive transformation to overcome the limitation of PFM that can only simulate diffusive transformations [19].

A lot of the models that are used in steel science research are empirical equations derived by fitting experimental curves. These models mostly provide information about the phase fractions and the kinetics of the transformations, but they do not give a complete description of the microstructure. In contrast, PFM can estimate phase fractions, element distributions, other essential aspects of the microstructure and even provide a three-dimensional (3-D) image of it [20].

PFM predicts the microstructural evolution by determining the interface movement of a microstructure considering the thermodynamics and the kinetics of the alloy [20]. Diffusion equations can also be solved simultaneously to predict the distribution of the elements in the microstructure [16]. The model is not a sharp interface model, which means that there is a finite area (or volume if the system is 3D) at the grain boundaries that belongs to both phases.

Another critical point that makes the implementation of the method complicated is that nucleation of a new phase is difficult to be defined. So, the nucleation rate and the preferable nucleation sites are mainly determined based on experimental data. Also, the prediction of interface movement is challenging to be done either theoretically or experimentally and often the interface mobility is used as a fitting parameter [20]. Usually, for the simulations of the Q&P process, carbide precipitation is suppressed even though simulations showed locally high carbon concentrations and these sites would be potential sites where carbides could precipitate [17].

1.4 Aim and structure of the thesis

This thesis aims to give insights into the effect of PAGS on the novel Q&P processing method using PFM. In chapter 2, the literature review is presented and the impact of PAGS on each step of the Q&P processing method is discussed. Specifically, the effect of PAGS on the kinetics of the martensitic transformation and the morphology of the resulting martensite is described, which is relevant to the first and the final quenching steps of the Q&P process. Then, the way that PAGS affects the carbon kinetics during partitioning is explained, together with the factors that control austenite thermal stability which is of great importance for the Q&P process. In chapter 3, a brief description of the phase-field modelling algorithm and its basic mathematical equations is given, and details about how the simulations were set to tackle the research questions are presented. In chapter 4, the outcome of the simulations is shown. In chapter 5, the discussion of the results is displayed, including a comparison to other research works. Finally, in chapter 6, the conclusions and suggestions for future research are presented.

Chapter 2

Literature review

In figure 2.1 the evolution of the microstructure during the Q&P process is illustrated. The white matrix is the austenite, the plates that are formed denote the martensite and the distribution of carbon during the steps is shown using a grayscale with a dark shade meaning a carbon-rich area.

The thermal stability of austenite is an essential aspect of the study of the Q&P process because it indicates the conditions that are required for austenite to be retained at room temperature. So, the main factors that govern the thermal stability of austenite are reviewed in this chapter. These factors will also help to the understanding of the effect of PAGS on austenite's stability during the Q&P process. Nevertheless, before that, it is essential to present the main equations that govern the martensitic transformation and the partitioning step.

For the martensite formation, the equations that estimate the resulting phase fractions with respect to the quenching temperature are presented, and those equations are relevant for the quenching taking place at T_Q temperature after austenitisation and at room temperature after partitioning as it is shown in figure 1.2.

For the partitioning step, the equations that determine the equilibrium phase fractions and the corresponding to those phases carbon content are also given in this chapter for the partitioning temperature T_p (figure 1.2).

Having reviewed the above, the effect of PAGS on the process, and the stability of austenite are discussed in this chapter. Finally, other studies done using phase-field modelling are reviewed since it is the tool that was also used for the present study.

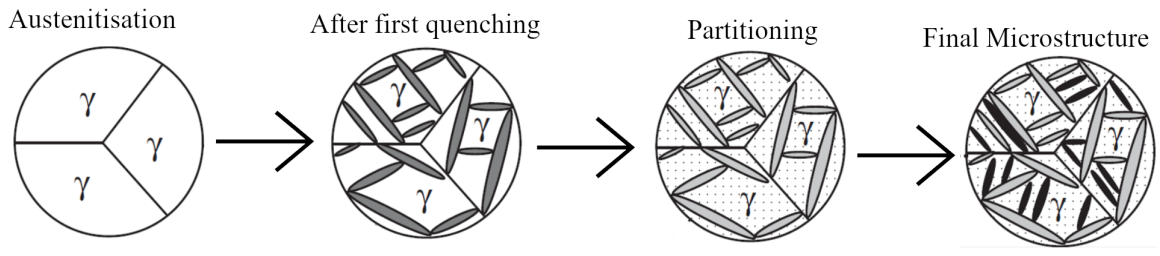

Figure 2.1: The microstructural evolution of steel that undergoes the Q&P process. The austenitic matrix and the martensitic plates that are formed after each quenching are illustrated. The grayscale indicates the carbon distribution on each step with the darker shades denoting a carbon-rich area.

2.1 Determination of the microstructural evolution during the Q&P process

2.1.1 First quenching

The prediction of the phase fractions resulting after the first quenching of the heat treatment (figure 1.2) is essential for the control of the microstructure and the modelling of the partitioning step that follows. After the first quenching of the fully austenitic microstructure at T_Q temperature, a controlled fraction of martensite is introduced in the microstructure. A widely used model for the determination of martensite phase fraction after quenching is the Koistinen and Marburger (K-M) equation [21] (equation 2.1.1) where T_Q is the quenching temperature and α_m can be expressed as a function of the chemical composition of the alloy (equation 2.1.2 where α_m is in K^{-1} and composition in wt. %) [22].

$$f_m = 1 - exp\{-\alpha_m(M_s - T_Q)\} \tag{2.1.1}$$

$$\alpha_m = 0.0224 - 0.0107C - 0.0007Mn - 0.00005Ni - 0.00012Cr - 0.0001Mo \tag{2.1.2}$$

The M_s temperature can be determined based on the composition of the alloy using an equation such as equation 2.1.3 (M_s in °C and composition in wt. %) [22].

$$Ms = 462 - 273C - 26Mn - 16Ni - 13Cr - 30Mo \tag{2.1.3}$$

2.1.2 Partitioning process

During partitioning, martensite and austenite coexist in the microstructure at T_P and this can give rise to a movement of the γ/α' interface. In order to determine the final phase fractions, it is important to investigate if any interface movement happens during partitioning that can change the phase fractions resulted after the first quenching step.

Santofimia et al. [23] investigated how the mobility of the γ/α' interface affects phase fractions and carbon partitioning by performing one-dimensional simulations. It was found that for very low interface mobility, the γ/α' interface was practically immobile and the retained austenite fraction depended on the quenching temperature. Consequently, for this case, an optimum quenching temperature can be calculated that

maximises the retained austenite content in the resulting microstructure after the final quenching.

Experimental work was done in another research using dilatometry to identify any volume changes during partioning [13]. No significant volume change was observed for steel of composition of 0.25C-2.5Mn-1.47Ni-1.01Cr (wt %) and partitioning duration relevant to commercial continuous production techniques. Moreover, in the same study, the volume of the retained austenite was found to be in agreement with the simulations performed considering low interface mobility. So, interface mobility can be neglected for the partitioning times and temperatures of this study and for alloys of similar composition.

The next step is to investigate how the phase fractions and the corresponding carbon concentrations are affected by the partitioning step. Speer et al. presented a model to describe the microstructural evolution of Q&P steels [1, 24]. To determine the fractions and the carbon content of the phases, they assumed constrained carbon equilibrium (CCE) conditions during partitioning that means that the γ/α' interface is immobile. At the same time, only carbon atoms can partition from martensite to austenite. Carbon is assumed uniformly distributed after the first quenching and its concentration is equal to the nominal composition due to the diffusionless nature of the martensitic transformation. Carbide precipitation and bainite formation are suppressed.

The mass balance of iron is given in equation 2.1.4. $f^{\gamma}_{before-P}$ is the austenite phase fraction before the partitioning step, while $f^{\gamma}_{after-P}$ and $X^{\gamma}_{after-P}$ are the phase fraction and the carbon concentration of austenite, respectively, at the end of partitioning and according to the CCE. Finally, X^{alloy} is the nominal carbon composition of the alloy. All the phase fractions and phase concentrations considering Speer's model are expressed in mole fractions.

$$f^{\gamma}_{after-P}(1 - X^{\gamma}_{after-P}) = f^{\gamma}_{before-P}(1 - X^{alloy}) \tag{2.1.4}$$

The total carbon content is given by equation 2.1.5 where $f^{\alpha}_{after-P}$ and $X^{\alpha}_{after-P}$ is the fraction and the carbon content of martensite after partitioning.

$$f^{\alpha}_{after-P}X^{\alpha}_{after-P} + f^{\gamma}_{after-P}X^{\gamma}_{after-P} = X^{alloy} \tag{2.1.5}$$

Moreover, the sum of the phase fractions of austenite and martensite must be equal to 1 (equation 2.1.6).

$$f^{\alpha}_{after-P} + f^{\gamma}_{after-P} = 1 \tag{2.1.6}$$

The CCE concentration of carbon at both sides of the γ/α' interface, at a specific partitioning temperature, is determined by assuming CCE conditions and using thermodynamical data. For the austenite/martensite system, the carbon concentrations are given in equation 2.1.7 where T_P is in K and R is the gas constant in $JK^{-1}mol^{-1}$. Equation 2.1.7 was derived experimentally by Lobo and Geiger by determining the activity of carbon in both phases and consequently, the carbon concentrations that result in the same chemical potential of carbon in both phases [25, 26].

$$X^{\gamma}_{after-P} = X^{\alpha}_{after-P} \cdot e^{\frac{76789-43.8T-(169105-120.4T)X^{\gamma}}{RT}} \tag{2.1.7}$$

By solving the above system of equations for given processing temperatures (T_Q and T_P), the phase fractions and the carbon content of each phase after partitioning can be determined. It is important to note that these values are the CCE values that means that the system has to remain at the partitioning temperature for long enough to reach them. The fact that the γ/α' interface is assumed to be immobile does not automatically imply that the phase fractions are constant since carbon atom movement is allowed and the mole fractions of the phases can change. Finally, this model was developed for the case of a binary alloy, but it is used for more complex systems.

The kinetics of carbon during partitioning can be described by Fick's second law that is shown in equation 2.1.8 for both phases (α' and γ). The diffusivity coefficient of carbon (D) is determined for each phase and it dependents on the carbon concentration of the corresponding phase [23, 27]. Numerical methods are found in the literature to solve the diffusion problem [28].

$$\frac{\partial X}{\partial t} = D\frac{\partial^2 X}{\partial x^2} \tag{2.1.8}$$

2.1.3 Final quenching

To model the final quenching, equation 2.1.3 can be used to estimate the new M_s temperature for the carbon enriched austenite with carbon content given by $X^{\gamma}_{after-P}$. If the new M_s temperature is below room temperature, austenite is retained at room temperature. Otherwise, austenite will transform to α' on the last quenching again according to equation 2.1.1. Provided that the fraction of martensite that is present during partitioning contains enough carbon to stabilise the austenite via the partitioning process, and if the partitioning time is not enough to homogenise the distribution of carbon in the austenite, then profiles of carbon concentration are evolving, making it essential to investigate austenite's stability locally. This means that especially for

short partitioning times or large austenite grains, part of an austenitic grain that is enriched in carbon can be stabilised and part of it that has not been enriched sufficiently in carbon will transform in martensite at the final quenching.

2.2 Factors determining the thermal stability of austenite

Stabilising austenite at room temperature is one of the main goals of the Q&P process. Before examining the effect of PAGS on the stabilisation process, it is essential first to investigate what are the factors that affect austenite's thermal stability. The ways that austenite is stabilised are of chemical and mechanical nature and they are discussed in this section

2.2.1 Chemical stabilisation

Austenite can be stabilised thermally if its local carbon concentration is high enough. So, the distribution of carbon in a microstructure that undergoes partitioning is of great importance determining the locations where austenite will be retained. Furthermore, Al and Si additions are used in the alloy to suppress cementite precipitation because carbide precipitation consumes carbon which is no longer available to stabilise the austenite [13]. Also Mn and Ni additions stabilise austenite at lower temperatures [29].

An optimal quenching temperature exists assuming CCE conditions. A model to determine this temperature has been proposed [30]. According to this model, the M_s temperature is calculated for the alloy based on the chemical composition using an expression such as equation 2.1.3. By varying the quenching temperature, the corresponding martensite fraction formed is determined using equation 2.1.1. By assuming that phase fractions of martensite and austenite do not change during partitioning and that carbon partitions to austenite following equation 2.1.7, the carbon content of austenite after partitioning can be known. Then, a new M_s temperature is calculated for the carbon-enriched austenite (equation 2.1.3) and equation 2.1.1 is used again to determine the possibility of formation of M_2 after quenching to room temperature for the T_Q that is examined. The above is repeated for a range of T_Q, aiming to maximise the content of retained austenite in the final microstructure.

The model above is described graphically in figure 2.2 for a microstructure consisting of 0.5 austenite and 0.5 ferrite that undergoes Q&P after intercritical annealing. The dashed lines show austenite and martensite fractions after the first quenching

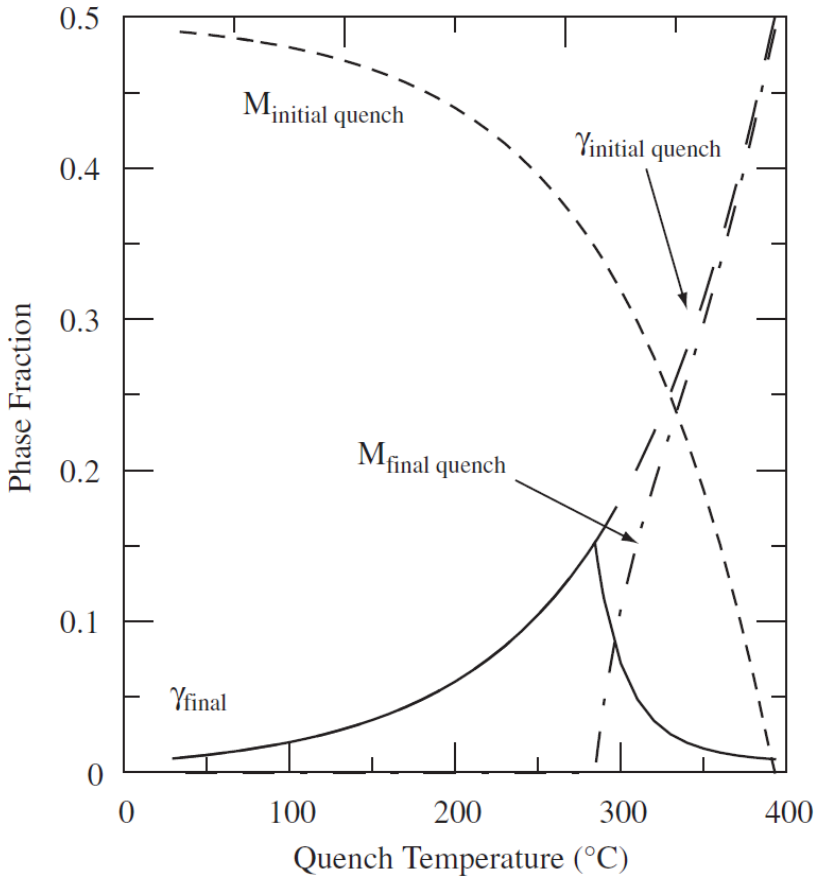

Figure 2.2: The dashed lines show austenite and martensite fractions after the first quenching as a function of the T_Q and the continuous line shows the retained austenite fraction of the final microstructure. The optimum quenching temperature is defined on the graph as the quenching temperature that maximises retained austenite content. This graph is for a 0.19C1.96Al1.46Mn0.02Si (wt %) steel that underwent intercritical annealing [1].

as a function of T_Q, and the continuous line shows the retained austenite fraction of the final microstructure. A peak is present because if the quenching temperature is relatively high, then there is not enough martensite to provide austenite with the carbon that is required and M_2 is formed. If the quenching temperature is relatively low, M_2 do not form but there is not much austenite left after the first quenching to get stabilised. So, there is an optimum quenching temperature that results in a maximum fraction of retained austenite.

Several methods have been used to determine the minimum required amount of carbon for austenite stabilisation at room temperature for a defined system with specific characteristics. Two approaches are presented here.

- Mecozzi et al. [16] did this calculation thermodynamically. They used available thermodynamic data to estimate the Gibbs free energy change for the non-diffusional transformation of austenite to martensite for a range of carbon com-

positions and temperatures. Moreover, for a fixed composition, the temperature that corresponds to a driving force that is equal to zero is the theoretical M_s temperature of the alloy. Finally, to estimate the carbon content that stabilises austenite the theoretical M_s temperature was set equal to the room temperature (so that austenite is stable at room temperature) and the carbon content that gives a driving force for non-diffusional transformation that is equal to zero was calculated. This carbon content is the critical value above which austenite is sufficiently enriched in carbon and is retained at room temperature after the final quenching.

- Another approach was used by Takahama et al. [17]. At this research paper, phase-field modelling simulation was employed to model the partitioning process. Having derived the carbon concentration maps after a fixed partitioning time, the critical carbon content value for stabilisation was used as a fitting parameter so that the martensite content that is introduced after the final quenching matches the prediction of the K-M equation (equation 2.1.1).

2.2.2 Mechanical stabilisation

It is known that the grain size of austenite affects its tendency to form martensite when temperature decreases [31]. Specifically, during the martensitic transformation, strain energy is induced to the microstructure due to the volume difference of α' and γ phases. The ability of the microstructure to accommodate this strain energy and the relaxation mechanisms that take place to achieve this are strongly related to the austenite grain size [32]. The material tries to minimise the strain energy during the martensitic transformation and two of the relaxation mechanisms that act in favour of the martensitic transformation are listed below.

- As the martensitic transformation progresses, new martensite nuclei are created repeatedly at the γ/α' interface. The fact that numerous new nuclei nucleate continuously at the γ/α' front, results in a reduction of the strain energy and it acts as a relaxation mechanism. This is known as the autocatalytic effect since it also enhances the kinetics of the transformation [33].

- During the martensitic transformation, plastic deformation is induced to the austenitic matrix so that a part of the transformation strain can be accommodated by austenite resulting in a reduction of the strain energy of the system. However, the accumulation of plastic deformation into austenite increases its stored energy and after a point the second relaxation mechanism can no longer

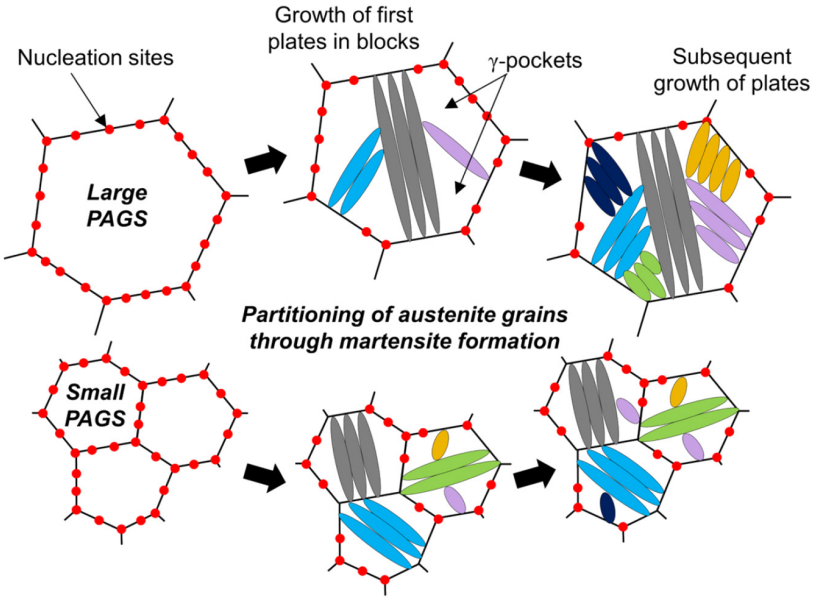

Figure 2.3: γ-Pockets forming during martensite formation that reduce the austenite grain size retarding the transformation [32]

contribute making the formation of martensite less favourable as the transformation progresses. [32].

The formation of martensite in an austenitic matrix results in continuous grain refinement of austenite by creating austenite-pockets as it can be seen in Fig. 2.3. As the transformation proceeds, the untransformed austenite increases its stored energy because the accumulation of plastic deformation reduces the effectiveness of the second relaxation mechanism [6]. Furthermore, it is known that the smaller pockets (and small austenite grains in general) cannot accommodate the strains efficiently and the strain energy cannot be minimised effectively [34]. Both phenomena increase the stability of austenite. As more austenite is consumed, the martensitic transformation becomes less energetically favourable and this is the reason that the transformation requires a continuously increasing undercooling to proceed. If the austenitic grains are sufficiently small, the transformation stops. This phenomenon is called mechanical stabilisation of austenite [12].

Finally, it is believed that film austenite is more stable than blocky austenite because as martensitic transformation occurs, it induces stresses to the surrounding austenite films that result in a hydrostatic pressure that enhances austenite stability [35].

To summarise the section considering austenite thermal stability, high carbon content and small austenite grain size increases austenite thermal stability and hinders the martensitic transformation.

2.3 The effect of prior austenite grain size on the Quenching and Partitioning process

In this section, the effect of PAGS on each step of the Q&P processing method is examined separately. Aspects such as the effect of PAGS on the transformations taking place and on the morphology of the final microstructure are presented.

2.3.1 Martensitic transformation

Martensite is affected significantly by PAGS variation in terms of size and morphology. Specifically, reduction of PAGS results in size reduction of the corresponding martensite packets and blocks, whereas little or no change was observed in lath size [6, 7, 12, 15, 36, 37]. Laths do not show noticeable variation in size with decreasing PAGS since their size is affected mainly by the carbon segregation at the lath boundaries [38]. However, laths show variation in shape. Lath morphology has been studied using electron backscatter diffraction and it was found that with decreasing PAGS, laths shape tends to be equiaxed and also their aspect-ratio probability distribution becomes wider [32]

Tataki et al. studied the effect of PAGS on the hierarchical martensitic structure. They investigated experimentally the martensitic microstructures resulted by coarse, fine and ultra-fine parent austenite grains [39]. The results showed that for coarse parent austenite grains, the martensitic laths exhibited a multi-variant transformation. So, the parent austenite was separated in multiple packets. The fine-grained and the ultra-fine parent austenite produced microstructures where laths grew in a single variant or in variants that have common habit plane. As a result, when austenite grain size was reduced significantly, parent austenite grains consisting of a single block of laths were found. The change of the hierarchical structure with decreasing PAGS is described schematically in figure 2.4.

An explanation for the reduction of the number of variants with decreasing PAGS is that when the PAGS is small, fewer laths nucleate compared to a material with large PAGS, so there are fewer chances for all the 24 Kurdjumov-Sachs orientation relationship to be observed. Since there is not enough space to have several laths nucleating at different sites simultaneously, the number of packets contained into a single grain is reduced [34].

The M_s temperature is a measure of the driving force that is needed for the martensitic transformation to initiate. It has been found that M_s and M_f temperatures decrease with decreasing PAGS [5, 12, 18, 32, 40, 41] so the whole transformation

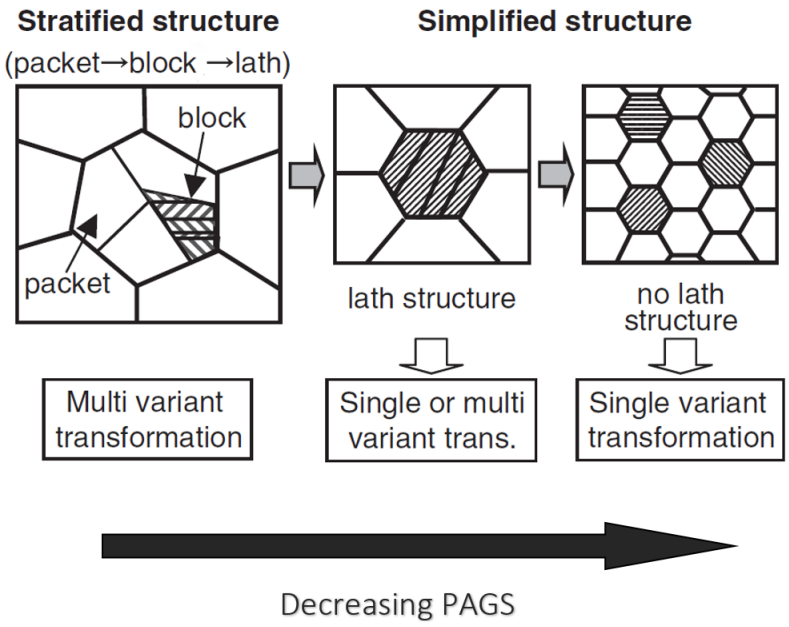

Figure 2.4: The transition from multivariant transformation to single variant transformation with decreasing PAGS; for very small PAGS, packets are not found and only parent austenite grains consisting of a block of laths are present [39]

is shifted to a lower temperature range. It is possible to obtain stable austenite at room temperature if the grains are sufficiently small to reduce Ms below room temperature [32, 41]. Nevertheless, other aspects such as the chemical composition affect the M_s significantly [8]. It is then important that the selection of the quenching temperature in the Q&P process is made taking also into account the PAGS because the shift of the M_s and M_f temperatures will affect the phase fractions at the final microstructure.

Considering nucleation, a multi-variant transformation has lower transformation energy. According to the theoretical calculations, it was found that a single variant transformation requires 17 times more transformation energy than a multi-variant transformation and this confirmed that the energy for transformation is increased with decreasing austenite grain size [39].

Considering the growth rate, Celada-Casedo et al. [32] explained that when PAGS is small, despite the fact that nucleation needs a high driving force, there are many possible nucleation sites compared to a material with large PAGS because of the increased grain boundaries density (figure 2.3). At the same time, the autocatalytic effect provides even more nucleation sites to the system. According to the experimental results, the transformation rate of a small-grained microstructure peaks when a martensitic fraction of about 0.3 has been formed and it remains higher up to the formation of a fraction of 0.6 of martensite. After that mechanical stabilisation takes

place and hinders the formation of martensite [39].

2.3.2 Partitioning

In the work done by Celada-Casero et al., the partitioning of carbon in microstructures with approximately the same phase fractions but with different PAGS was examined [12]. In order to achieve the same phase fractions, different quenching temperatures were used for specimens with different PAGS to account for the change of M_s with the austenite grain size.

According to this research, partitioning was more efficient in the small grain microstructures because the two phases (austenite and martensite) where more homogeneously distributed than in coarse-grained specimens. This makes partitioning more efficient since there is a larger α'/γ total interface where carbon partitioning can occur. Furthermore, for small PAGS, it takes less time for the carbon to enrich and homogenise in austenite because carbon has to diffuse shorter distances.

Experimental results also showed that microstructures with large PAGS exhibit also wider grain size statistical distributions. This makes the partitioning process more complex because the variety of austenite grain sizes also results in different carbon enrichment among the austenite grains, which has an impact on the mechanical stability of the austenite. The variety of grain sizes also makes the control of the partitioning process difficult for microstructures with large PAGS.

The experimental study of Celada-Casero et al. [12] is the basis of the simulations done in this work and it is discussed thoroughly in the rest of this thesis.

2.3.3 Competing mechanisms

Carbon can get trapped at defects such as dislocations making partitioning less efficient [42]. Experiments showed that small PAGS increases the dislocation density of the resulting martensite [6] due to the high strength of austenite. In addition, the increasing interface area resulting from the size reduction of the PAGS, packets and blocks, creates interfaces where carbon also can be trapped at [43].

Bainitic transformation is also possible during partitioning. Luo et al. [44] proposed that a critical PAGS exists below which the bainitic transformation is suppressed. According to another research, the same mechanism that stabilises austenite mechanically is responsible for the delay or suppression of the bainitic transformation since the small austenitic grains cannot accommodate the strain energy occurring from the bainitic transformation [45].

Finally, carbides can precipitate after quenching and during partitioning. Martensitic microstructures resulted from large austenite parent grains exhibit carbides due to auto-tempering [6]. During partitioning, relatively high temperatures or long times may also give rise to carbide precipitation [46]. Carbide precipitation happening in any stage of the Q&P process consumes carbon that otherwise would be available to stabilise austenite.

2.4 Phase field modelling of the quenching and partitioning process

Phase-field modelling is a computationally intensive model and so it is common to prefer two-dimensional simulations (2D) over three-dimensional simulations (3D) to reduce the computational load. Simulations of the Q&P process showed that 2D simulations represented adequately the experimentally observed microstructures. The same was also found for the 2D microstructures obtained by producing cross-sections of a 3D simulation. However, in the 3D model, diffusion can occur in three directions instead of two, and carbon can diffuse faster in the microstructure during partitioning. Despite the difference between 2D and 3D models, results from both models showed good agreement with the experimental data [16].

2.4.1 Martensitic transformation

Yeddu studied martensitic growth by performing phase-field modelling simulations taking into account the stress field that evolves in the austenite and martensite due to the transformation [18].

For the case of small PAGS, results confirmed that martensite grows on a single crystallographic direction due to the preference of martensite to grow towards the direction that minimises the elastic strain energy of the system. Nevertheless, the fact that martensite grows along a single direction makes the accommodation of the transformation stresses difficult and a high driving force is needed for nucleation which is in agreement with the findings of Tataki et al. [39].

The plastic strain for a fine-grained microstructure was found to be relatively low at the beginning of the transformation because it is more difficult for a material with small grains to undergo plastic deformation compared to a material with large grains. However, at the end of the transformation, the plastic strain was increased because the other relaxation mechanisms (section 2.2.2) could not help further to the accommodation of the strain energy and plastic deformation had become the primary

relaxation mechanism.

In contrast, when PAGS is large, the minimisation of the transformation stresses gives rise to the multivariable transformation mechanism that was introduced by Tataki et al [39].

Moreover, for large PAGS, the plastic strain is high at the onset of the transformation because the material can be deformed plastically easier than a fine-grained material. So, initially, plastic deformation is the dominant relaxation mechanism.

A more simple way to simulate martensite is to represent it as acicular ferrite. To do that, a fully austenitic microstructure is selected as initial microstructure and an appropriate nucleation model is selected that define the possible nucleation sites and the nuclei density. A cooling rate is selected and the simulation starts. By defining the anisotropy between the two phases properly, ferrite nuclei grow having an acicular shape as they were martensitic blocks. The martensitic transformation is simulated as a diffusive transformation to overcome the limitations of phase-field modelling and get microstructures similar to the austenite/martensite microstructures observed experimentally. Then the resulted microstructure can be used as the initial microstructure for a simulation of carbon partitioning [16]. This approach will be used in this thesis.

2.4.2 Partitioning of carbon

According to the PFM simulations performed by Mecozzi et al. [16], the diffusion of carbon from martensite to austenite during short partitioning times creates a concentration gradient inside the austenitic grains, with the outer region of the grain enriched in carbon compared to the inner area (Figure 2.5). If the material is quenched at this point, the outer region of the grain will be stabilised at room temperature while the inner area will be transformed to martensite creating martensitic islands surrounded by austenite. This is true especially for short partitioning times or for relatively large grains because carbon may not have enough time to diffuse in the whole austenite grain. Consequently, smaller austenite grains have the ability to obtain a high carbon content in their interior even after short partitioning times which makes stabilisation more efficient.

2.4.3 Final quenching step

It is important to determine the minimum amount of austenite carbon content that is required to stabilise austenite at room temperature for the system that is examined. This can be done with one of the methods that were described already in section 2.1.1.

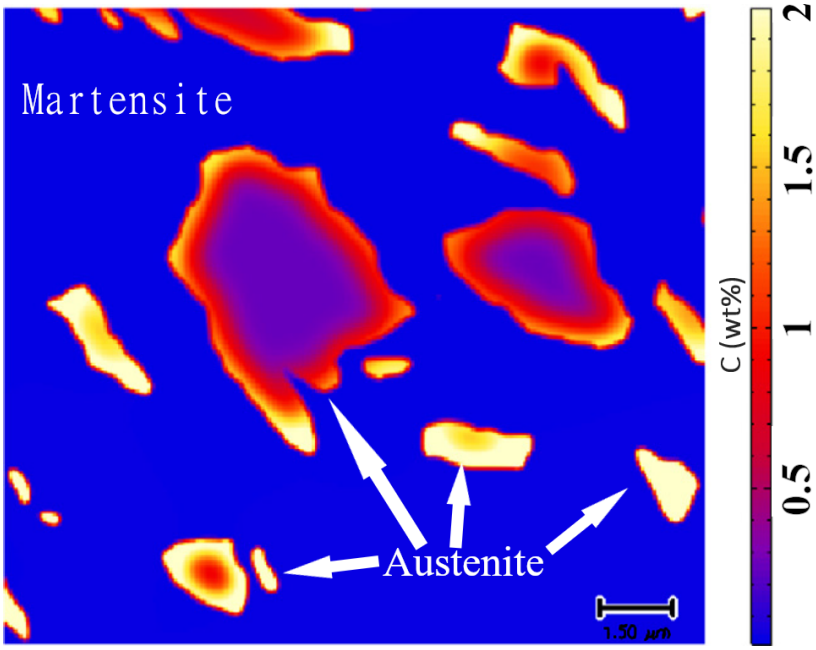

Figure 2.5: A map produced by PFM that shows carbon concentration on a microstructure after partitioning for 100 s at 400°C. The carbon gradient in austenite grains during partitioning is shown; small grains are enriched in carbon, and their profile is more homogeneous compared to large austenite grains [16].

Then, having calculated the map that shows the carbon distribution in austenite (such as in figure 2.5) and with the critical carbon content for stabilisation known, the austenite that is sufficiently enriched in carbon is retained and the rest transforms to M_2. By doing this, a final representation of the final microstructure, the corresponding phase fractions, and the carbon distribution can be derived for the case that is studied [16, 17].

2.5 Summary

The effect of prior austenite grain boundaries size on the Q&P process and the resulting microstructure was reviewed. The importance of considering PAGS as a design parameter during the design of the Q&P was highlighted and the main conclusions are listed below.

- High carbon content and small grains size increases austenite thermal stability and vice versa.
- Martensitic transformation is shifted to lower temperatures with decreasing PAGS since a higher undercooling is required for the transformation to start. The transformation is initially faster in a microstructure with small austenite grains due to the abundance of nucleation sites at the grain boundaries.

However, the transformation rate decreases at a later stage, because of the phenomenon of the mechanical stabilisation.

- The size of martensitic packets and blocks decrease with decreasing PAGS while laths do not show a significant change of size. The number of different variants that are present in a single packet also reduces with decreasing PAGS.
- Partitioning is found to be more efficient in fine-grained microstructures because it takes place at a larger area of γ/α' interface. Furthermore, the shorter distance that carbon has to diffuse makes homogenisation faster.
- Mechanisms such as carbide precipitation and bainite formation can occur during Q&P and affect the final microstructure. Small PAGS can contribute to the suppression of both mechanisms.
- Phase-field modelling was found to be a useful tool for the investigation of the Q&P process because it can give insights into the mechanisms evolving during the treatment that are difficult to be observed experimentally.

2.6 Research Questions

The distribution of carbon during partitioning affects austenite stability significantly. However, it is difficult to observe experimentally how carbon is redistributed during partitioning and the use of a PFM becomes appealing for this type of studies. In the present study, in order to investigate the effect of PAGS on the microstructural evolution and the carbon kinetics during the process of Q&P, PFM is used. Specifically, investigating the effect of PAGS on:

- The austenite grain size statistical and spatial distribution resulting after the first quenching, and how the distribution of grain sizes affects the partitioning process and the final microstructure.
- The time that is required for austenite to be sufficiently enriched in carbon during partitioning.
- The mechanical stability of the austenite in the final microstructure and the TRIP effect.

Chapter 3

Simulations

3.1 The phase-field model

The model that was used for the simulations is based on the works of Steinbach et al. [47] and Eiken et al. [48], and it is the same model that was also used to simulate the Q&P in the works by Mecozzi et al. [16] and Takahama et al. [17]. The MICRESS© software was employed to perform the simulations [49].

To perform a phase-field simulation, a simulation domain is selected and an initial microstructure is set. Each grain of the microstructure is characterised by a phase-field parameter $\phi_i(\vec{r},t)$ that defines whether the point of the simulation domain positioned by the vector $\vec{r}$ at the time t belongs to the grain i ($\phi_i(\vec{r},t)=1$) or not ($\phi_i(\vec{r},t)=0$). The values of $\phi_i(\vec{r},t)$ change gradually from 1 to 0 at the boundaries between neighbouring grains, creating what is called a diffuse interface. This is the reason why the phase-field model is not a sharp interface model.

The molar fraction of the solutes is defined by $x_i^{k=1...\xi}$ where ξ is the number of the solutes, i denotes the corresponding grain and x^0 is the molar fraction of the solvent. Within the diffuse interface, the conservation of the total number of moles per unit volume is given by equation 3.1.1, where ν is the number of the grains that participate in the interface that is examined.

$$x^k(\vec{r},t)=\sum_{i=1}^{\nu}\phi_i x_i^k(\vec{r},t) \tag{3.1.1}$$

The total energy of the system consists of two parts, the interfacial and the chemical energy. The interfacial energy is a function of the gradient of the phase-field parameters at the diffuse interface, while the chemical energy is a function of the phase-field parameter and the corresponding molar fraction of the solute and it refers to the free energy of the bulk. In equation 3.1.2, $F(\{\phi_i\},\{x_i\})$ is the total energy of the system, $f^{intf}(\{\phi_i\})$ and $f^{chem}(\{\phi_i\},\{\nabla\phi_i\})$ are the interfacial and the chemical free energy respectively.

$$F(\{\phi_i\},\{x_i\})=\int_A f^{intf}(\{\phi_i\},\{\nabla\phi_i\})+f^{chem}(\{\phi_i\},\{x_i\})dA \tag{3.1.2}$$

The simulation aims to minimise the total free energy of the system, The phase-

field parameters are calculated in every time step according to equation 3.1.3, where $\vec{n}$ is the vector that is normal to the interface with respect to the coordinate system of the growing grain, $M_{ij}^{\phi}(\vec{n})$ is the mobility of the interface and $\sigma_{ij}(\vec{n})$ the interface energy between grains i and j. $\Delta G_{ij}(\vec{x_i}, \vec{x_j}, T)$ is the thermodynamic driving force.

$$\dot{\phi}_i = \sum_{j \neq i}^{\phi} M_{ij}^{\phi}(\vec{n}) \left[b\Delta G_{ij}(\vec{x_i}, \vec{x_j}, T) - \sigma_{ij}(\vec{n}) K_{ij} + \sum_{i \neq j \neq k}^{\nu} J_{ijk} \right] \tag{3.1.3}$$

Also, b is a scaling factor of the driving force that is given in equation 3.1.4, K_{ij} is the pairwise curvature term (equation 3.1.5) and J_{ijk} accounts for the triple junctions of the system (equation 3.1.6), η is the thickness of the diffuse interface.

$$b = \frac{\pi}{\eta} \sqrt{\phi_i \phi_j} (\phi_i + \phi_j)) \tag{3.1.4}$$

$$K_{ij} = \frac{1}{\nu} \left(\nabla^2 \phi_i - \nabla^2 \phi_j \right) + \frac{\pi^2}{\nu \eta^2 (\phi_i - \phi_j)} \tag{3.1.5}$$

$$J_{ijk} = \frac{1}{\nu} \left(\sigma_{jk} - \sigma_{ik} \right) \left(\frac{\pi^2}{\eta^2} \phi_k + \nabla^2 \phi_k \right)_{ij} \tag{3.1.6}$$

The concentration terms $\vec{x_i}$ in equation 3.1.3 have to be determined on each simulation step. Therefore, equation 3.1.3 is coupled with the diffusion equations that are given in equation 3.1.7 and 3.1.8 where D_i^{kl} is the diffusivity (k is the diffusing component and l is the gradient component in grain i). $M_i^{ch,km}$ is the chemical mobility matrix and $f_i(\vec{x_i})$ the free energy density in grain i.

$$\frac{\partial x^k}{\partial t} = \nabla \sum_{i=1}^{\nu} \sum_{l=1}^{\xi} \phi_i D_i^{kl} \nabla x_i^l \tag{3.1.7}$$

$$D_i^{kl} = \sum_{m=1}^{\xi} M_i^{ch,km} \frac{\partial f(\vec{x_i})}{\partial x_i^m x_i^l} \tag{3.1.8}$$

The Thomson-Gibbs effect that accounts for the impact of the interface curvature on the total free energy of the phase is expressed in equation 3.1.9 [50]. υ is the interface velocity, M is the interface mobility, ΔG is the driving force of the transformation, σ is the interfacial energy and κ is the curvature of the interface. This equation defines the way in which the interfaces will move and subsequently the shape of the grains of the microstructure. For the case of Q&P simulations where the displacive martensitic formation is simulated as a diffusional acicular ferrite formation, the equation was used to optimise the shape of the martensitic blocks according to

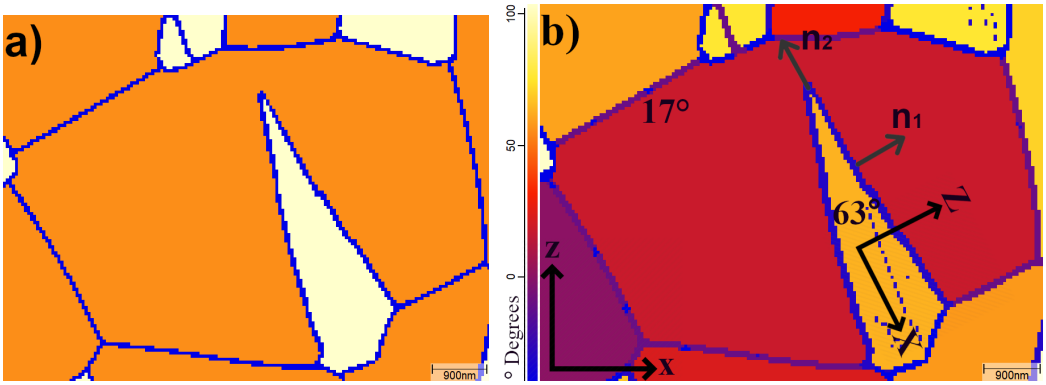

Figure 3.1: (a) An example of an austenitic microstructure where martensite (in white) is being formed. (b) Orientation map that shows the angles that define the orientation of every single grain. The two coordination systems are shown, one that is the global one and the second one that is the local coordinate system of the grain that is growing. $\vec{n_1}$ and $\vec{n_2}$ are the vectors normal to the α'/γ interface and they are essential for the definition of the anisotropy of the growth of the phase that is being formed.

the experimental results that were available [12].

$$v = M(\Delta G - \sigma\kappa) \tag{3.1.9}$$

When anisotropic phases are used in the simulations such as in the case of austenite/ferrite pair, the anisotropy between the phases has to be defined [16]. The presence of anisotropic phases leads to the dependence of the interfacial energy and mobility on the orientation of the vector that is vertical to the moving interface.

In figure 3.1(a), an austenitic grain of an Fe-C alloy is shown in orange. This grain undergoes a transformation from fcc to bcc and a block of ferrite has already been formed (in white colour). Each grain has a specific orientation that in 2D simulations is defined by a single angle. In figure 3.1(b), the angle of orientation of every grain is shown. The orientation angle is the rotation angle of the global coordinate system (figure 3.1 (b)) in order to be aligned with the local orientation system of the grain that grows. The bcc grains are always formed at an angle of $\pm 45°$ with the parent fcc grain. The unit vector $\vec{n}$ is defined normal to the interface with respect to the coordinate system of the growing grain. Two example normal vectors are drawn in figure 3.1, $\vec{n}_1$ and $\vec{n}_2$. The anisotropic functions $\alpha^{M,\sigma}$ are used to define the mobility and the interfacial energy of an interface accounting for the anisotropy.

Equations 3.1.10 and 3.1.11 show how the anisotropic functions $\alpha^{M,\sigma}$ correct the mobility and the interfacial energy according to the orientation of the normal to the interface vector $\vec{n}$.

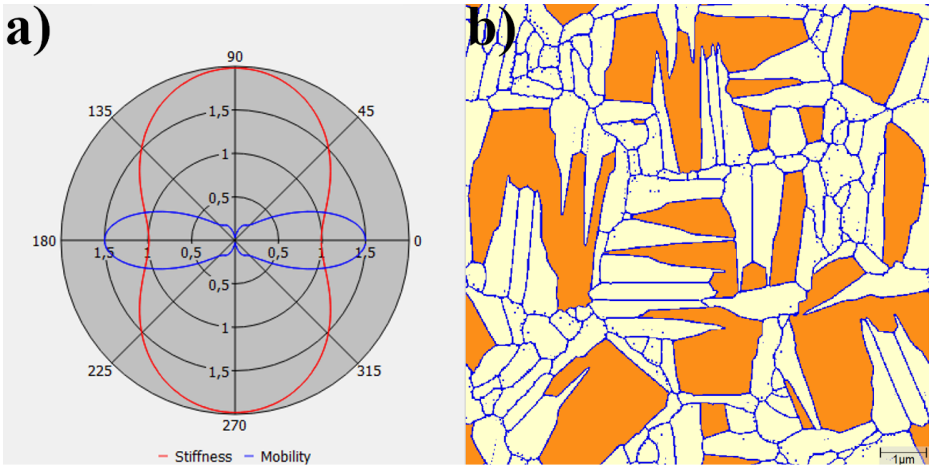

Figure 3.2: (a) Interfacial energy and mobility pole figure of an strongly anisotropic fcc/bcc interaction (b) that results in the growth of columnar ferritic grains in the microstructure

$$M^{\phi}_{\alpha\gamma}(\vec{n}) = M^{\phi 0}_{\alpha\gamma}\alpha^{M}(\vec{n}) \tag{3.1.10}$$

$$\sigma^{\phi}_{\alpha\gamma}(\vec{n}) = \sigma^{\phi 0}_{\alpha\gamma}\alpha^{\sigma}(\vec{n}) \tag{3.1.11}$$

The tetragonal anisostropy functions $\alpha^{M}(\vec{n})$ and $\alpha^{\sigma}(\vec{n})$ are shown in equations 3.1.12 and 3.1.13. The parameters δ_1 δ_2 are used to control the anisotropy.

$$\alpha^{M}(\vec{n}) = [1 + 4\delta_1^{M}(n_x^4 + n_y^4 + n_z^4 - 0.75)](1 - n_z^2 - \delta_2^{M} n_z^2) \tag{3.1.12}$$

$$\alpha^{\sigma}(\vec{n}) = [1 - 4\delta_1^{\sigma}(n_x^4 + n_y^4 + n_z^4 - 0.75)](1 - n_z^2 - \delta_2^{\sigma} n_z^2) \tag{3.1.13}$$

In figure 3.2 an example of a strongly anisotropic fcc/bcc interaction is shown. These graphs were produced by setting appropriate values for the coefficients δ_1^{M}, δ_2^{σ} and δ_1^{M}, δ_2^{σ} from equations 3.1.12 and 3.1.13 respectively. There is a clear preference for the ferritic grains to grow towards a specific direction that is defined by their orientation angle. For a close to isotropic interaction such as that in figure 3.3, the grains tend to be equiaxed.

A linearised phase diagram was used for the determination of the driving force for fcc to bcc transformation [16, 49]. The transformation is assumed that occurs under para equilibrium conditions where substitutional alloying elements do not diffuse and a linearised phase diagram can describe the transformation. A linearised Fe-C phase diagram that is suitable for this type of calculations is shown in figure 3.4. The use of linearised phase diagrams instead of thermodynamical databases, when it is possible,

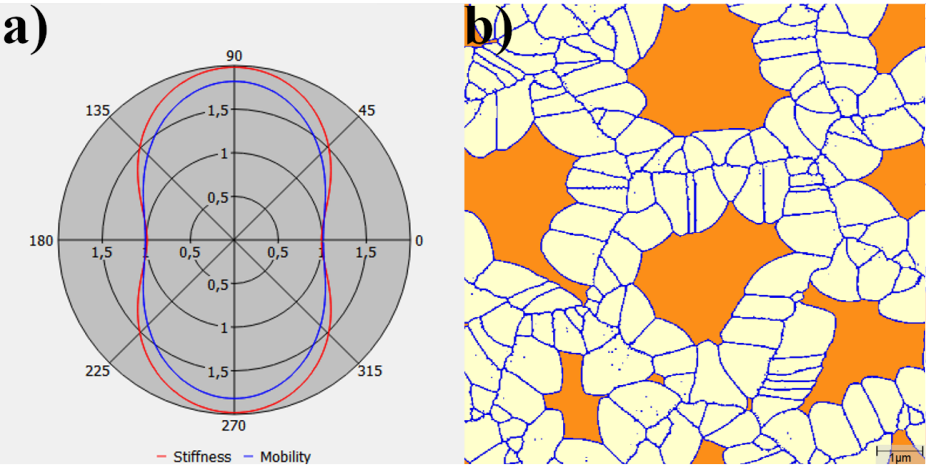

Figure 3.3: (a) Interfacial energy and mobility pole figure of a close to isotropic fcc/bcc interaction (b) that results in the growth of close to eqiuaxed ferritic grains in the microstructure

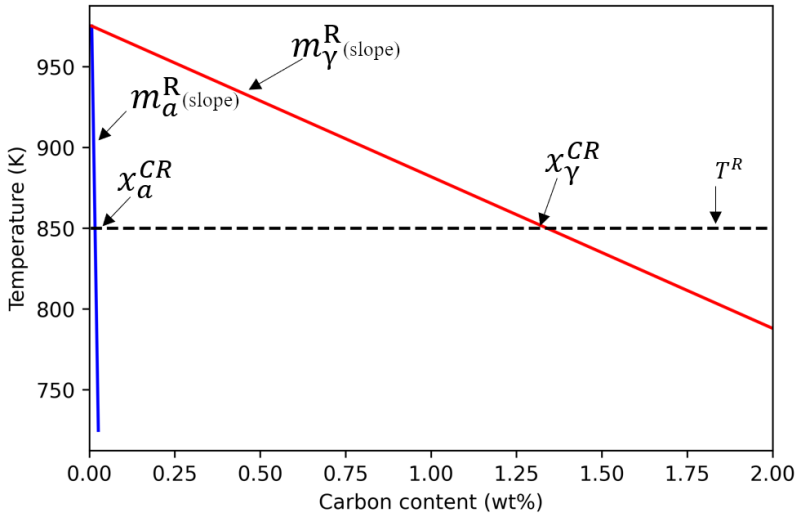

Figure 3.4: Linerised Fe-C phase diagram that was used for the simulations.

reduces the computational load of the algorithm. The driving force is a function of the undercooling and it is given by equation 3.1.14.

$$\Delta G_{\alpha\gamma}(x_\alpha^C, x_\gamma^C, T) = \Delta S \Delta T \tag{3.1.14}$$

The undercooling ΔT is calculated by equation 3.1.15, where x_α^C and x_γ^C are the local carbon content of austenite and martensite respectively while x_α^{Ceq} and x_γ^{Ceq} are the equilibrium values predicted by the linerised phase diagram (figure 3.4). m_α^R and m_γ^R are the slopes of the linerised lines shown in figure 3.4.

$$\Delta T = \frac{1}{2}\left[m_\alpha^R(x_\alpha^C - x_\alpha^{Ceq}) + m_\gamma^R(x_\gamma^C - x_\gamma^{Ceq})\right] \tag{3.1.15}$$

The ΔS is given by equation 3.1.16 below that determines an average value of

Table 3.1: Chemical composition of the studied alloy [12]

C (wt. %)	Mn (wt. %)	Si (wt. %)	Mo (wt. %)	Fe (wt. %)
0.2	3.5	1.5	0.5	balance

Table 3.2: The quenching temperature of the first quenching and the experimental phase fractions of the final microstructures for PAGS of 6 and 67μm

PAGS (μm)	T_Q	M_1	Bainite	RA	M_2
6	225	0.83	0.02	0.13	0.02
67	260	0.80	0.03	0.14	0.03

ΔS for the temperature range between the austenite to ferrite equilibrium transition temperature T_γ^{eq} and the experimentally measured M_s temperature.

$$\Delta S = \frac{\Delta G(M_s)}{T_\gamma^{eq} - M_s} \tag{3.1.16}$$

3.2 Reference experimental data

The experimental data presented in the work of Celada-Casero et al. [12] was used in the simulations. In that work, the microstructural development during the application of the Q&P process as a function of PAGS was investigated in a steel with the composition given in table 3.1. The same composition is studied in the present work. The cases of PAGS of 6, 25, and 67 μm were selected from the available experimental data to perform the simulations.

The quenching temperature is set each time considering the effect of PAGS on the M_s temperature and aiming to produce microstructures of a fraction of approximately 0.80 of martensite after the first quenching step. Furthermore, the quenching step was followed by partitioning at 400°C for 50 s and finally, quenching to room temperature.

The evolution of the martensite phase fraction with the temperature during quenching is presented in figure 3.5 for the three PAGS selected in this work. Figure 3.5 highlights that M_s decreases with increasing PAGS. The M_s temperatures are 323, 334 and 349 C° for the PAGS of 6, 25 and 67 μm, respectively. In table 3.2, the phase fractions of the microstructures of different PAGS for each step of the process are presented (data for PAGS of 25μm was not available).

The final microstructures that had undergone Q&P were studied using electron back-scattered diffraction (EBSD) and results are shown in figure 3.6. Martensitic grains are equiaxed for small PAGS while they tend to be columnar with increasing PAGS. Moreover, austenite is in the form of blocks that tend to be more elongated with

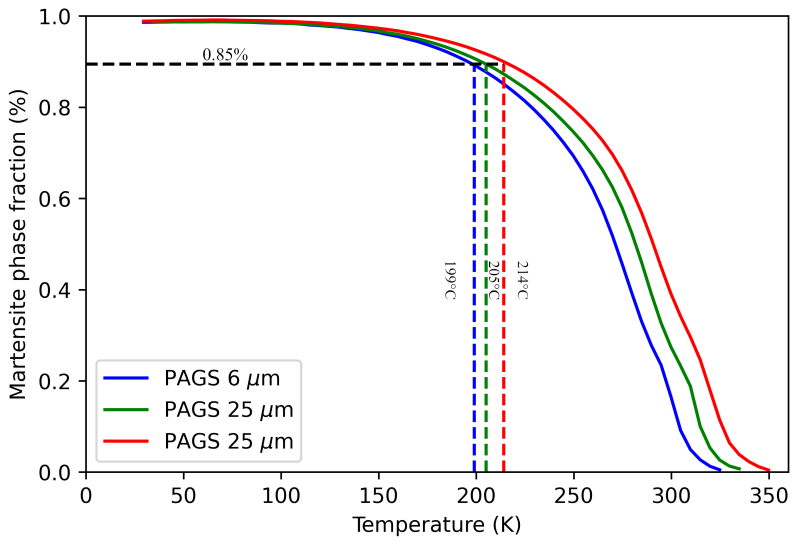

Figure 3.5: Martensitic phase fraction versus temperature, during quenching, for the three microstructures of different PAGS that were examined.

Table 3.3: RA and M1 grain size for the three PAGS measured by EBSD.

PAGS (μm)	6	25	67
RA grain size (μm)	0.2	0.32	0.33
M1 grain size (μm)	1.1	6.3	10.6

increasing PAGS. The average RA and martensite grain size for each microstructure of different PAGS is shown in table 3.3. In the experiments, almost all the austenite was retained. It is assumed that no significant interface movement occurred according to experimental results for a steel of about the same composition and partitioning conditions [13]. So, the grain size of the RA is also representative of the austenite grain size right after the first quenching.

3.3 Simulations Conditions

The simulation scheme that was followed is depicted in figure 3.7. Three initial austenitic microstructures of different grain sizes were created artificially by the software. The simulation starts at the M_s temperature of each microstructure. A fraction of approximately 0.895 of martensite is introduced to the microstructures. To achieve that, different quenching temperatures are selected to account for the different austenite grain sizes (figure 3.5). Then, the microstructures of the quenching simulations are used as input for the partitioning simulation that follows but the carbon distribution is reset to 0.2% wt. for both phases which is the nominal composition. Lastly, When partitioning had finished, the final quenching was simulated, but this time

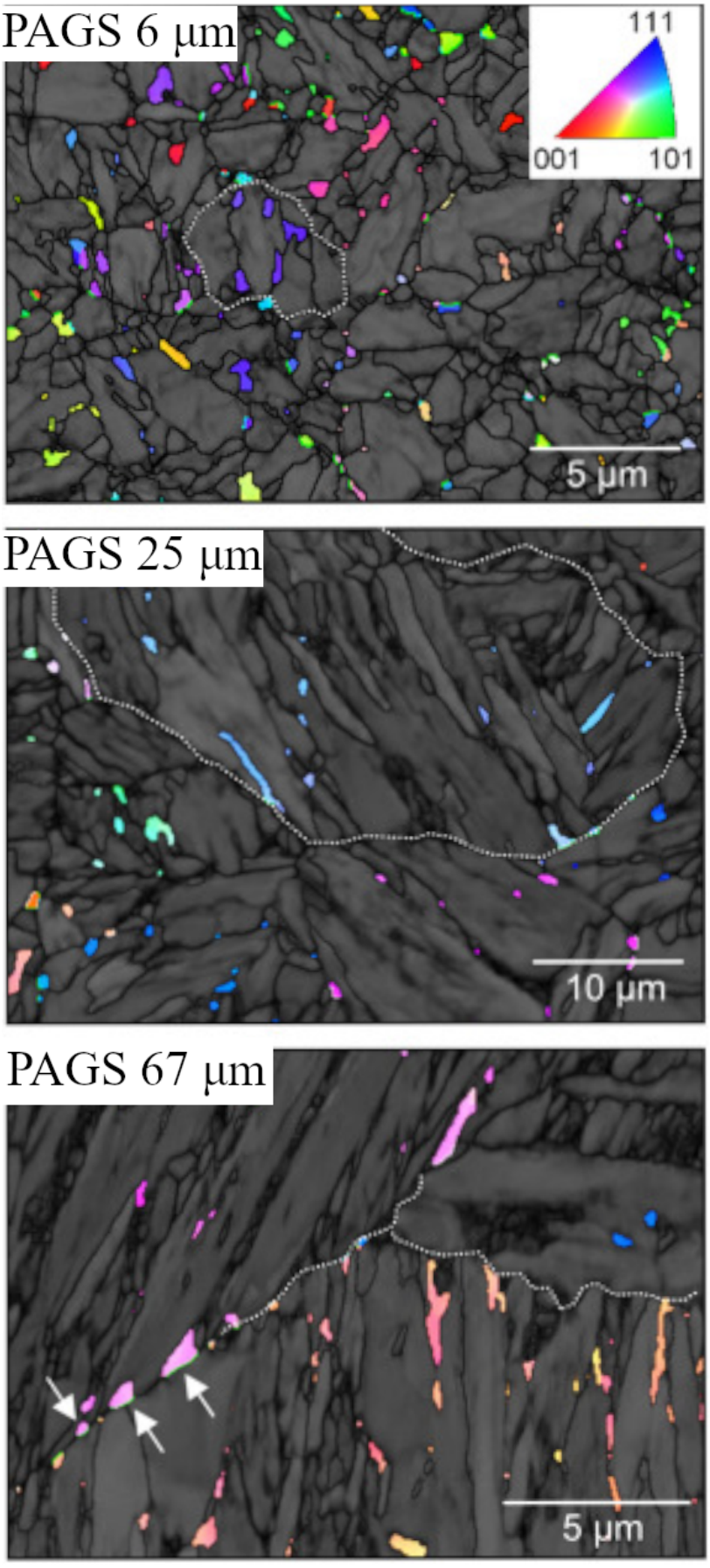

Figure 3.6: EBSD images for the three different PAGS. The pole figure indicates the texture of austenite [12].

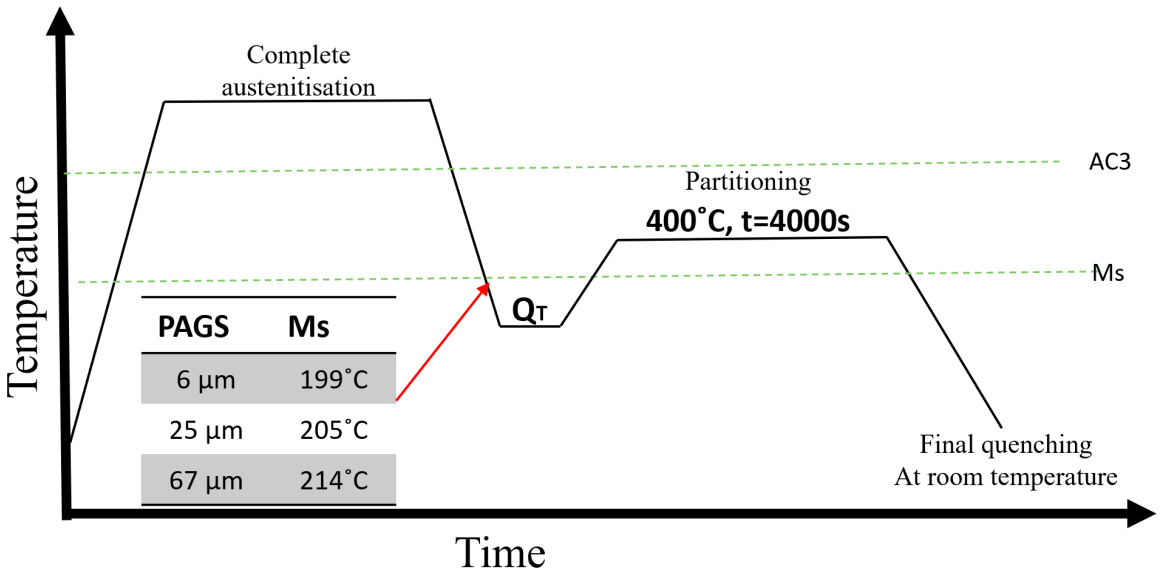

Figure 3.7: The scheme that was used for the simulation. The simulations start at the beginning of the first martensitic transformation and the quenching temperatures are selected aiming to create microstructures with phase fractions of 0.105 of austenite and 0.895 of martensite. Partitioning follows for 4000 s and the simulations end with the final quenching to room temperature.

PFM was not used. The final simulation is based on the local examination of the carbon distribution resulted after the partitioning simulation that shows if austenite was sufficiently enriched in carbon at a local level. The three simulation steps (first quenching, partitioning, and final quenching) are discussed extensively in this section.

3.3.1 Austenitisation

The austenitic microstructures of the different PAGS were created in MICRESS©. A round shape was selected for the grains. Then, a minimum and a maximum radius were selected to create a grain size distribution. Those limit values were $\pm$ 1 μm from the selected PAGS value. With the allowed radius range being defined, seeds are placed randomly in the simulation domain and a Voronoi construction lead to the microstructure.

For the cases of PAGS of 6 and 25 μm, 57 austenitic grains were set at the initial microstructure. To accommodate these grains, domains of sizes 40x40 and 80x80 μm were created respectively. For the case of 67 μm, 5 grains were selected and the dimensions of the domain were 133x133 μm. The above characteristics of the initial microstructures domains are summarised in table 3.4. The domains with the initial austenitic microstructures are shown if figure 3.8.

The grid spacing was 0.05 μm for all the quenching simulations (table 3.4). This value is a compromise between simulation speed and image resolution of the simulated

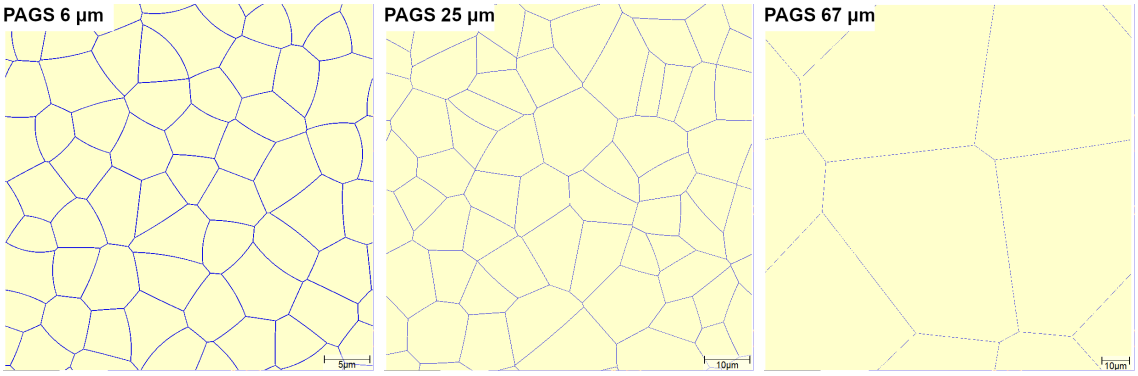

Figure 3.8: The three different initial microstructures used for the simulation of the Q&P process

Table 3.4: The domains of the initial austenitic microstructures used for the quenching simulations

PAGS	6 μm	25 μm	67 μm
Number of grains of initial microstructure	57	57	5
Domain size	40x40 μm	80x80 μm	133x133 μm
Grid spacing	0.05 μm	0.05 μm	0.05 μm
M_s	323°C	334°C	349°C
Q_T	199°C	205°C	214°C

microstructures. Periodic boundary conditions were set for the diffusion and the phase-field equations for all the simulations.

3.3.2 Quenching

The simulations aimed to produce microstructures consisting of fractions of 0.105 austenite and 0.895 ferrite with the latter representing the M1 martensite (figure 1.2). The fraction of 0.105 austenite is selected because lower values would result in fine microstructures due to the continuous grain refining of austenite that would be difficult to be studied because of the resolution of the simulations. Larger values would lead to unrealistic microstructures that would consist of a high fraction of block austenite while in reality, a large fraction of that austenite would be in the form of film austenite. Film austenite with thickness less than 100 nm is challenging to be simulated because a very high simulation resolution is required making the computational load significantly larger. Therefore, film austenite is not considered for the simulations of this work.

The interface mobility of the α'/γ interface was used as a fitting factor to match the results of martensite formation from dilatometry experiments. The anisotropy between the two phases controls the way that ferrite grows into the austenitic matrix.

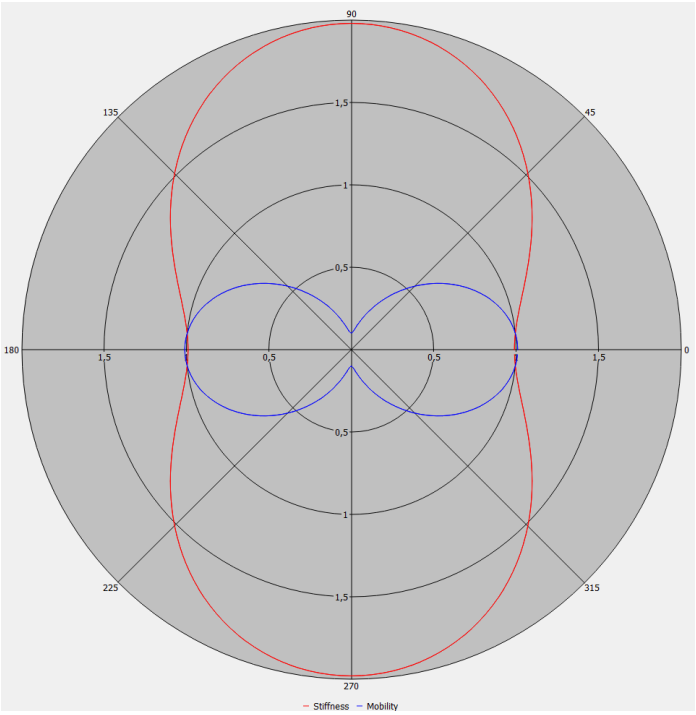

Figure 3.9: Interfacial energy and mobility pole figure of the quenching simulation

Table 3.5: The values of the linerised phase diagram at 850 K

$T^R(K)$	$x_\alpha^{CR}(wt\%)$	$x_\gamma^{CR}(wt\%)$	$m_\alpha^R(Kwt\%^{-1})$	$m_\gamma^R(Kwt\%^{-1})$	$\Delta S(J/(cm^3K))$
850	0.0166	1.3398	-13019.87	-93.94	0.67

To achieve a good representation of the experimental microstructure shown in figure 3.6 the anisotropy that is defined by the graph in figure 3.9 was selected. This anisotropy model was produced by selecting the values 0.01 and 0.1 for the δ_1^M and δ_2^M respectively that correspond to the mobility (equation 3.1.12). The values of 0.01 and 2 were selected for δ_1^σ and δ_2^σ respectively that correspond to the interfacial energy (equation 3.1.13).

The transformation is governed by a linearised phase diagram as that in figure 3.4 with the data from table 3.5.

The way that the model introduces the martensitic nuclei into the austenitic microstructure is based on the undercooling of the system as the temperature of the simulation decreases. No thermal gradient is present and latent heat is not considered, so the temperature is the same in the whole extend of the simulation domain. Seeds are placed at the pre-defined type of nucleation sites and the new nuclei have an initial size distribution that follows a pre-defined statistical distribution. A minimum required undercooling for nucleation is set for all the types of seeds and then, based on the radius of each seed, the extra undercooling (if it is needed) for every individual seed to nucleate is calculated by the software.

Initially, about two seeds per grain were placed in the grain boundaries of the fully austenitic microstructure for the three cases of different PAGS that were examined. The seeds were allowed to nucleate and grow until they meet an obstacle such as another grain boundary or another martensitic grain coming from another nucleus. This was done because as it is observed experimentally and as it is described graphically in figure 2.3, the first blocks that are created tend to grow across the parent grain resulting in austenite grain partitioning. Then, secondary nucleation was allowed to happen to introduce more martensitic nuclei, but this time nucleation in both fcc/fcc and fcc/bcc interfaces was permitted. The nuclei that are introduced at the second stage will also grow for as long as they do not find an obstacle. At a later stage, more and more nuclei are introduced in both types of interfaces until the microstructure is entirely transformed to martensite. For the partitioning simulations of the present thesis, the quenching simulations were stopped when a fraction of 0.895 of α' had been formed with the rest of the microstructure being untransformed austenite (0.105); these were the phase fractions used for the partitioning simulations. The steps of this scheme are depicted in figure 3.10 where the evolution of the microstructure with respect to the temperature is shown. The total number of the nuclei that are introduced on each step and the time in between the repeated nucleations was tuned aiming to achieve an adequate representation of the microstructures that were observed experimentally by Celada-Casero et al. [12]. Specifically, the total number of nuclei was used to match the grain size of martensite of the simulation with the experimentally measured values in table 3.3.

3.3.3 Partitioning

The microstructures produced by the quenching simulations for each PAGS examined with phase fractions of 0.105 γ and 0.895 α' are used as initial microstructures to perform the partitioning simulations. The carbon concentration is 0.2% wt. for both phases. The partitioning was done at 400°C and for 4000 s to see the whole evolution of the partitioning phenomenon. Intermediate partitioning times can be investigated. For each partitioning simulation, the same domain size as of the parent quenching simulation was used. However, a higher resolution (spacing of 0.04 μm) was selected to get more detailed carbon distributions within small grains.

An equation of Arrhenius type was used to calculate diffusion of carbon with the diffusivity being determined by Thermocalc© that was coupled to MICRESS©. To reduce calculation load, the average austenite concentration in carbon was considered to determine the diffusivity without considering the local carbon distribution. The diffusivity at 400°C for the three cases that were examined is shown in figure 3.11.

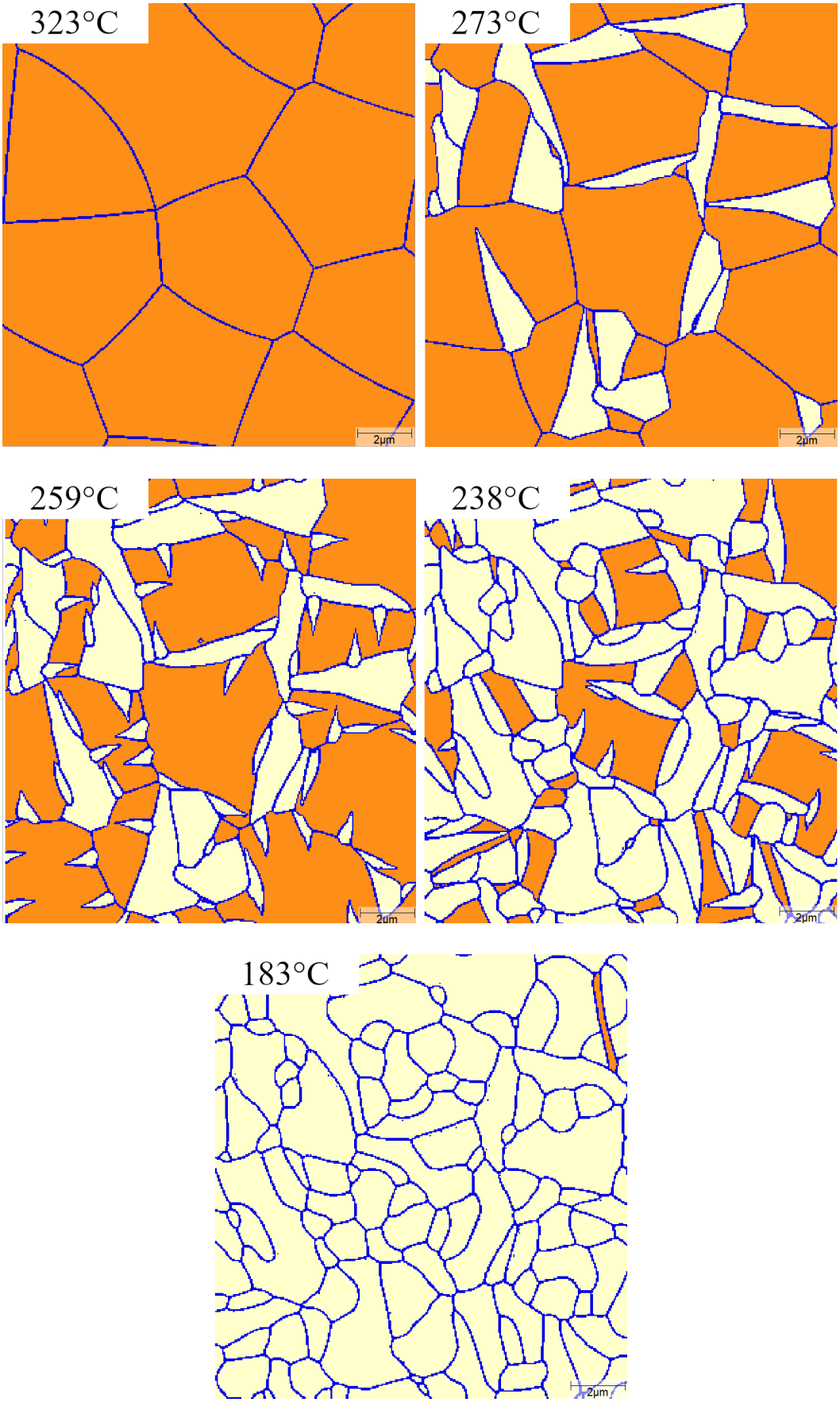

Figure 3.10: The evolution of the microstructure of PAGS of $6\mu m$ that undergoes quenching. Initially, nucleation takes place at the γ/γ interface and a few blocks of martensite grow across the austenitic grain. Later, nucleation happens also on the α'/γ interface.

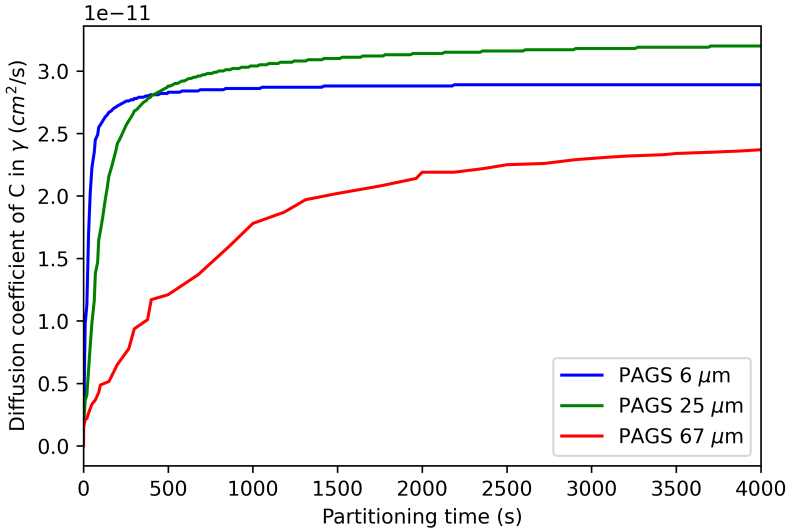

Figure 3.11: The carbon diffusion coefficient in austenite is affected by the carbon content, given enough partitioning time the carbon content is stabilised and the diffusion coefficients exhibit a plateau

Table 3.6: Kinetic parameters of the partitioning simulation

Kinetic Parameters			
Interface	α/α	γ/γ	γ/α
$M^0(m^4J^{-1}s^{-1})$	$2 \cdot 10^{-15}$	10^{-15}	10^{-15}
Interafacial energy (Jm^{-2})	10^{-10}	$2 \cdot 10^{-15}$	$2 \cdot 10^{-5}$

The different way that austenite gets enriched in carbon leads to different diffusivity with partitioning time for each case. The diffusivity for all the simulations reaches a plateau after some time when the average carbon content in austenite does not change significantly.

The same linearised phase diagram that was used for the determination of the driving force for the martensitic transformation (figure 3.4 and table 3.5) is used to determine the CCE conditions that govern the partitioning process. Kinetic parameters for the simulation of partitioning are shown in table 3.6. An immobile γ/α' interface is assumed during partitioning.

3.3.4 Final Quenching

To simulate the final quench, the amount of carbon content that is required to stabilise austenite at room temperature must be determined. In section 2.2.1, the thermodynamical calculations done by Mecozzi et al. [16] for the alloy of the present study was described. That study showed that 1.2 % wt. of carbon is required in austenite for stabilisation. Experimental work done by Celada Casero et al. [12] indicated that

the minimum carbon concentration measured in the RA was found to be 0.85% and it was assumed that this is the minimum amount of carbon for stabilisation. This difference in the critical carbon content between the theoretical calculations and the experimental data can be explained by the effect of manganese in austenite's stability. For the present work the value of 0.85% is selected as the critical for stabilisation value.

Chapter 4

Results

In this section, the results of each step of the simulation of the process are presented for the three cases of different PAGS.

For every PAGS that was examined, a microstructure with phase fractions of martensite and austenite of approximately 0.895 and 0.105 respectively was created through the quenching simulation. Then, this microstructure was used as input microstructure for the simulation of the step of partitioning.

The evolution of carbon distribution after 50,100,1000 and 4000 s of partitioning at 400 C° is presented for every PAGS. The colour scale of the results of the partitioning simulation is restricted to 0-3% wt. A few areas with significantly higher carbon content were present for short partitioning times but the maximum value of 3% was set for an easier interpretation of the results. The long partitioning time was selected to have a full description of the partitioning process that will help the understanding of carbon kinetics. Lastly, for comparison with the experimental data of Celada-Casero et al. [12], the final microstructure is illustrated for the case of partitioning for 50 s and quenching to room temperature for every PAGS. The three different phases that coexist are indicated (M1, RA, M2).

However, in the simulations, the phase fraction of austenite right before partitioning was about 0.105 while in the experiments was approximately 0.20 as it is reported in table 3.2.

4.1 PAGS of 6 μm

For PAGS equal to 6 μm the simulation domain was 40x40 μm. To make an easy comparison of the results with the other PAGSs, and taking advantage of the periodic boundary conditions, the domain is translated in both directions producing a domain of 80x80 μm.

In figure 4.1 (a-d) the evolution of the martensitic transformation during the first quenching is shown. Initially, the microstructure is fully austenitic (figure 4.1 (a)), at a lower temperature the first martensitic nuclei grow dividing the parent austenite grains into pockets (figure 4.1 (b)). Then, secondary nucleation takes place, new grains appear that also grow until they find a barrier such as a grain boundary or another grain. In figure 4.1 (d) the transformation is almost done. The microstructure in figure 4.1 (c) is selected to be used as input for the partitioning simulation. This microstructure corresponds to fractions of approximately 0.015 of austenite and 0.985 of martensite.

In figure 4.2 the austenite grain size distribution after the first quenching is presented. The mean grain size value is 0.74 μm and the standard deviation is 0.63 μm

In figure 4.3 (a-d) the carbon distribution after partitioning at 400°C for 50 100 1000 and 4000 s is illustrated. For short partitioning times as in the case of 50 s (figure 4.3 (c)), the small grains of the microstructure have already been enriched in carbon in their full extent, while in the cores of the large grains, carbon concentration has not been increased yet. After 1000 seconds all the grains are enriched in carbon but there is still some variation in the carbon content among the grains. After 4000 s figure (4.3 (d)) the distribution of carbon becomes even among the austenitic grains.

The carbon content distribution resulting after partitioning for 50 s at 400°C is selected to determine the microstructure after the final quenching at room temperature. The critical carbon value for stabilisation is 0.85% wt. for all the simulations and the final microstructure is shown in figure 4.4. The small grains of the microstructure managed to get stable even for the short partitioning time of 50 s while the large grains that did not manage to get enriched in their full extend formed martensitic islands on their centres. The final phase composition is 8.41% of RA, 89.45% of M1 and 2.09% of M2.

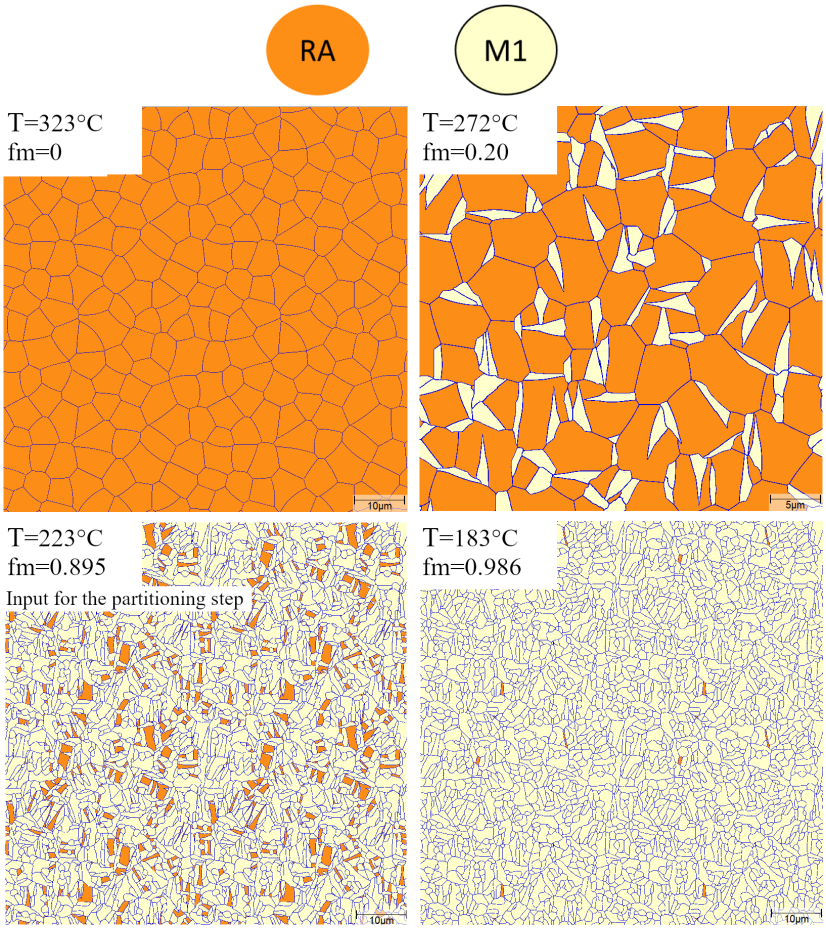

Figure 4.1: Quenching simulation for the case of PAGS of 6 μm

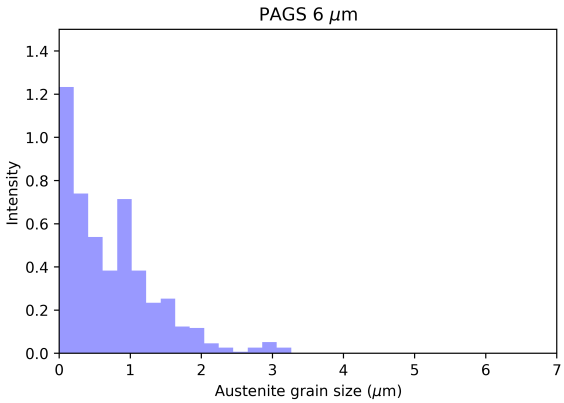

Figure 4.2: Grain size distribution of austenite after the first quenching for PAGS of 6 μm.

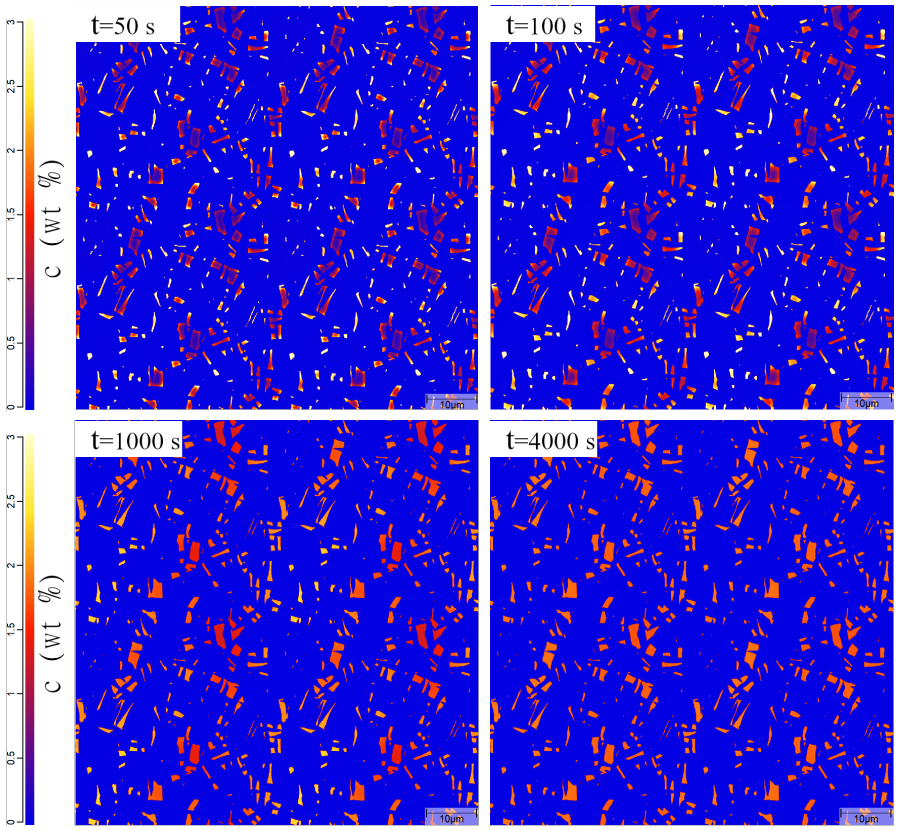

Figure 4.3: Carbon distribution from the partitioning simulation for the case of PAGS of 6 μm

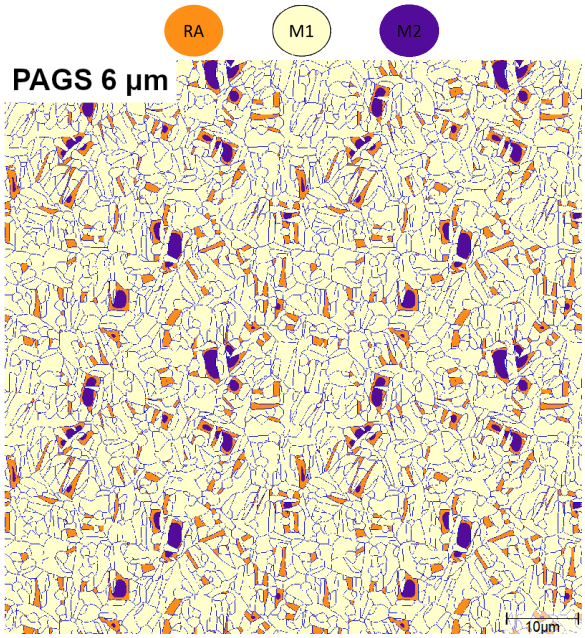

Figure 4.4: The final microstucture after partitioning for 50 s and quenching to room temperature for the case of PAGS of 6 μm

4.2 PAGS of 25 μm

The results of the quenching simulation for PAGS of 25 μm are shown in figure 4.5 (a-d). The domain size of the simulation is 80x80μm. Similarly, as in the case of PAGS of 6 μm about 2-3 martensitic blocks per austenitic grain nucleate on the γ/γ interface. The microstructure in figure 4.1 (c) is selected to be used as input for the partitioning simulation because it corresponds to fractions of approximately 0.105 of austenite and 0.895 of martensite. It is already apparent that austenite is coarser compared to the previous case.

The austenite grain size distribution right before partitioning is shown in figure 4.6. The distribution confirms the coarser austenite. The mean grain size value is 1.48 μm and the standard deviation is 1.48 μm

In figure 4.7 (a-d) the carbon distribution after partitioning at 400°C for 50 100 1000 and 4000 s is depicted. After 100 s of partitioning (figure 4.7 (b)), only the outer area of the grains has been enriched in carbon while the inner area still has the nominal composition of the alloy (0.2 % wt) with the exception of some very small grains that are visible in the figure. Even after 4000 s of partitioning the carbon concentration has not been homogenised yet and the carbon concentration varies among the grains.

The carbon content distribution resulting after partitioning for 50 s at 400°C is selected to determine the microstructure after the final quenching to room temperature 4.8. Most of the austenite grains did not have enough time to get enriched in carbon and they formed martensitic islands at the final quenching with the large parent austenite grains of the microstructures now consisting mainly of martensite. However, some small austenite grains still managed to get completely stable at room temperature and they are present in the final microstructure. The final phase composition is 4.88% of RA, 89.79% of M1 and 5.33% of M2.

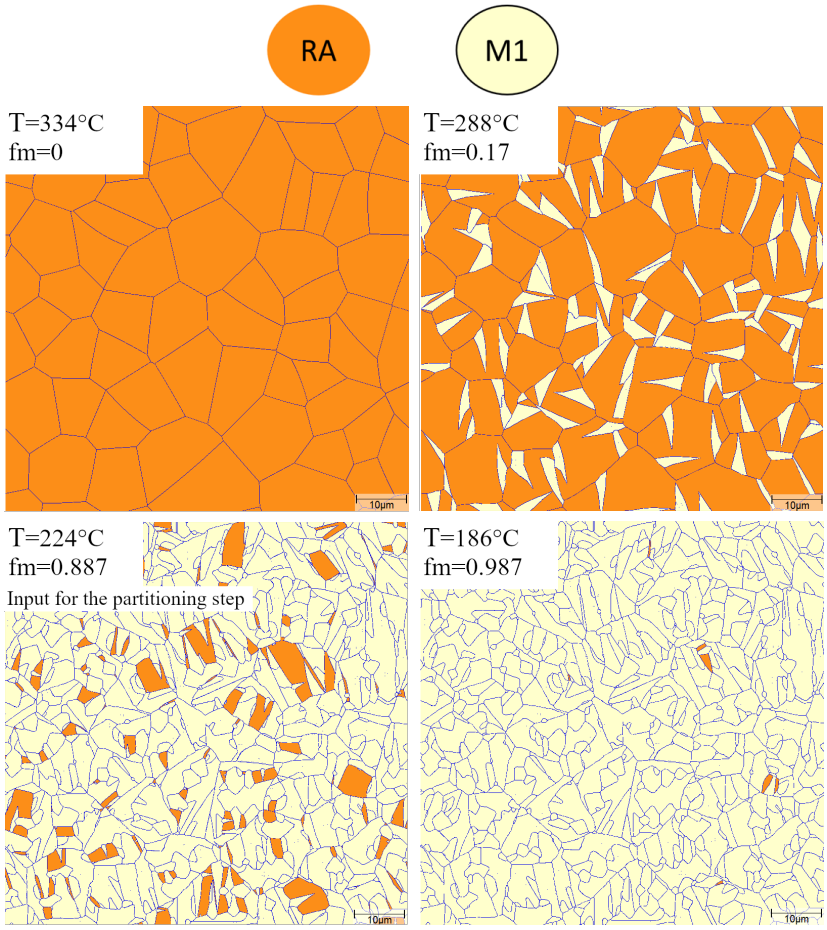

Figure 4.5: Quenching simulation for the case of PAGS of 25 μm

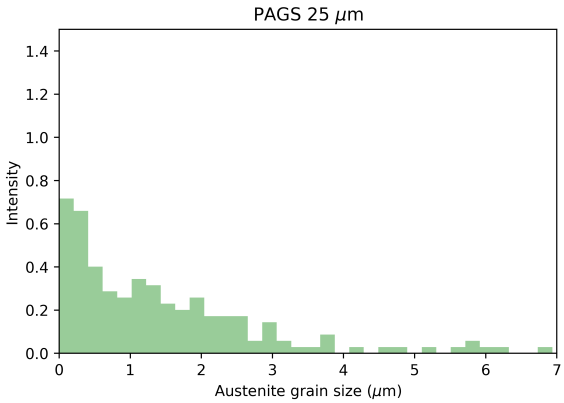

Figure 4.6: Grain size distribution of austenite after the first quenching for PAGS of 25 μm.

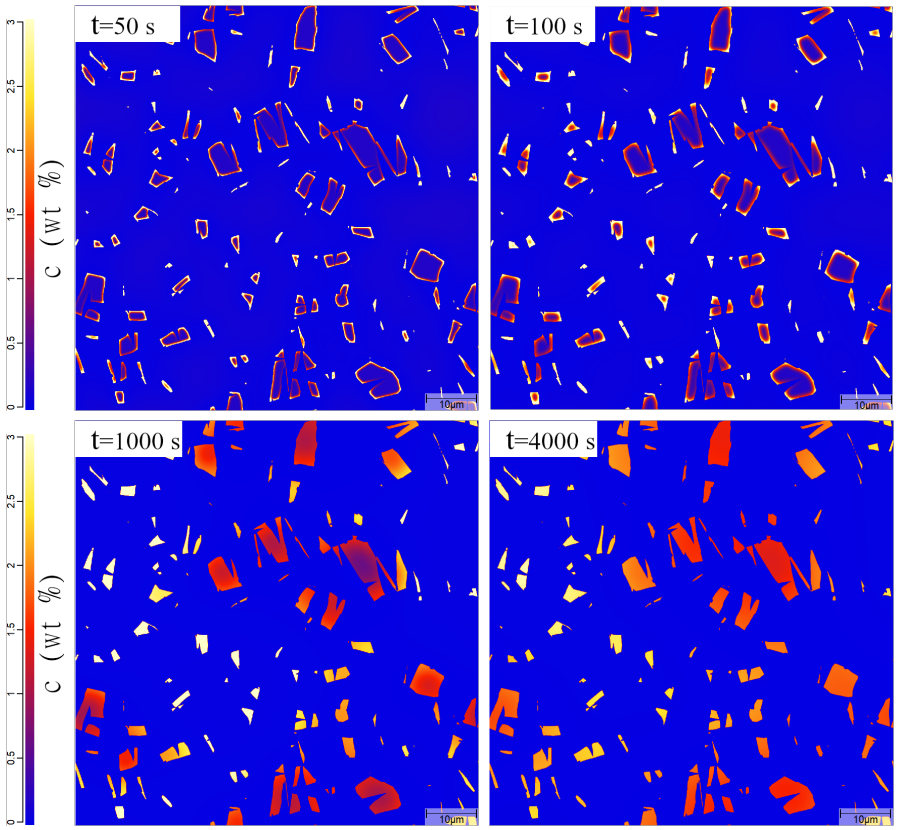

Figure 4.7: Carbon distribution from the partitioning simulation for the case of PAGS of 25 μm

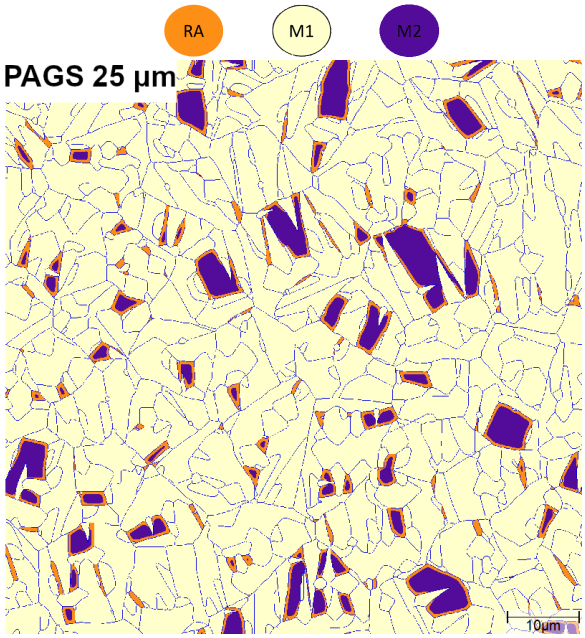

Figure 4.8: The final microstucture after partitioning for 50 s and quenching to room temperature for the case of PAGS of 25 μm

4.3 PAGS of 67 μm

Finally, the progress of the martensitic transformation is shown in figure 4.9 (a-d) for a PAGS of 67 μm, resulting in a microstructure that is significantly coarser. Large variations exist in the grain size of the martensitic blocks, with the ones that nucleated early being significantly larger. The odd shape that the remaining austenite has in figure 4.9 (c) is due to the recent nucleation of new martensitic blocks at the γ/α' interphase. The new grains had not had enough time to grow across their parent grain. The microstructure in figure 4.1 (c) is selected to be used as input for the partitioning simulation. Again, the phase fractions are approximately 0.105 for austenite and 0.895 for martensite.

The austenite grain size distribution right after the first quenching is shown in figure 4.10. The distribution is significantly wider compared to the previous cases. The mean grain size value is 2.15 μm and the standard deviation is 2.49 μm.

The results from the partitioning step are shown in figure 4.11 (a-d). Even after 4000 s (figure 4.11 (d)) the cores of the large grains of the microstructures have not increased their carbon content and they still have a concentration equal to approximately the nominal composition (0.2% wt). However, some small grains exhibit a very high carbon concentration.

The final microstructure after partitioning for 50 s at 400°C and quenching to room temperature is presented in figure 4.12. Almost every austenitic grain formed large martensitic islands at the final quenching. A narrow area of austenite that is close to the γ / α interface was able to remain stable at room temperature. The final phase composition is 2.3% of RA, 89.2% of M1 and 8.5% of M2.

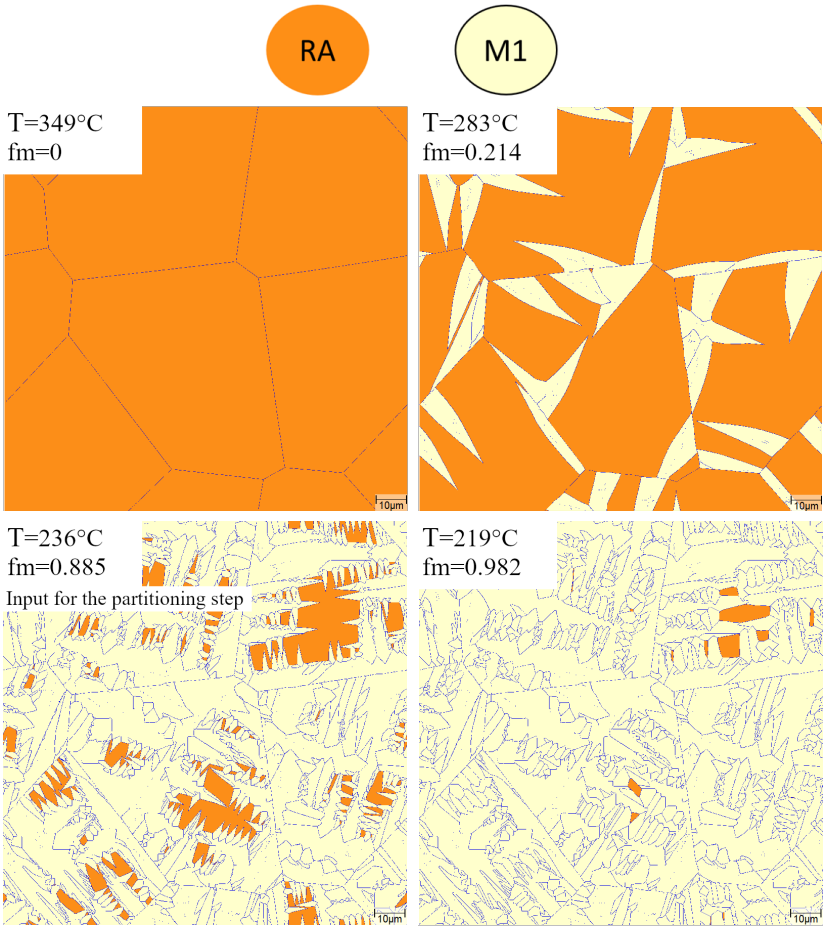

Figure 4.9: Quenching simulation for the case of PAGS of 67 μm

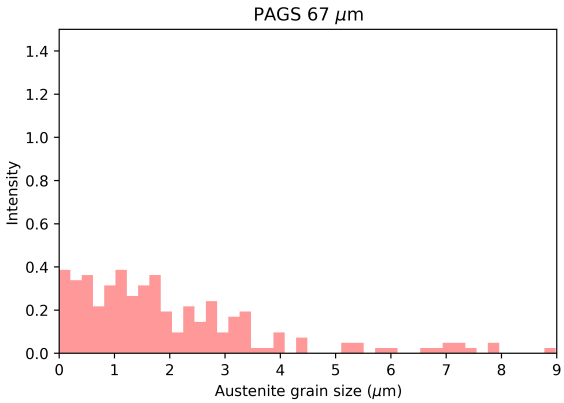

Figure 4.10: Grain size distribution of austenite after the first quenching for PAGS of 67 μm.

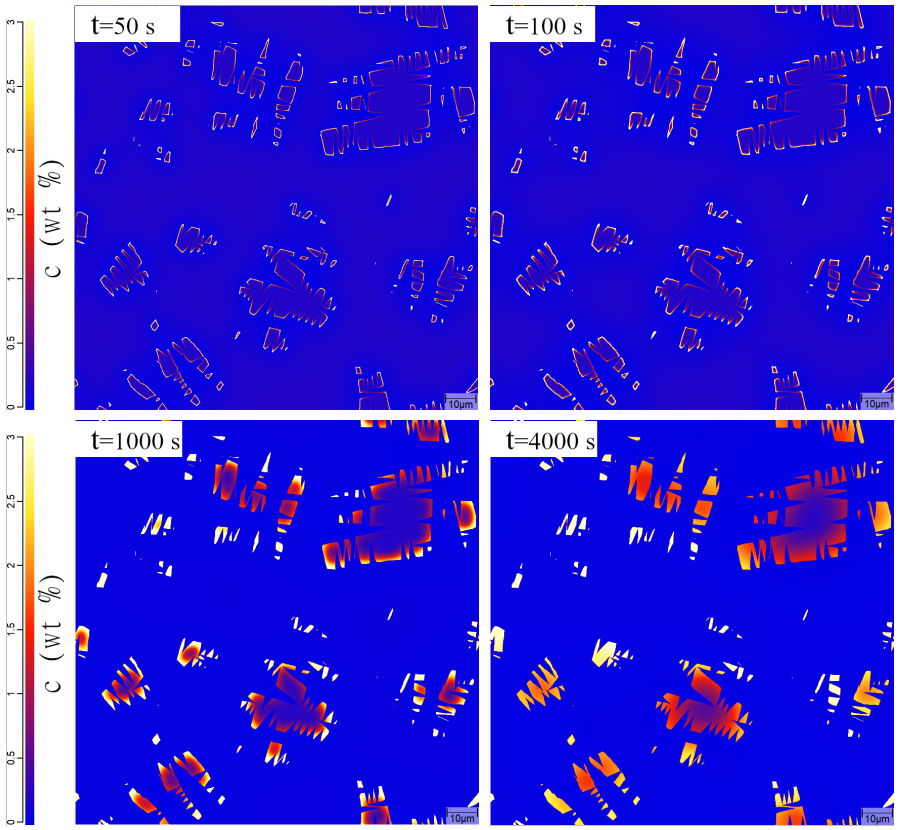

Figure 4.11: Carbon distribution from the partitioning simulation for the case of PAGS of 67 μm

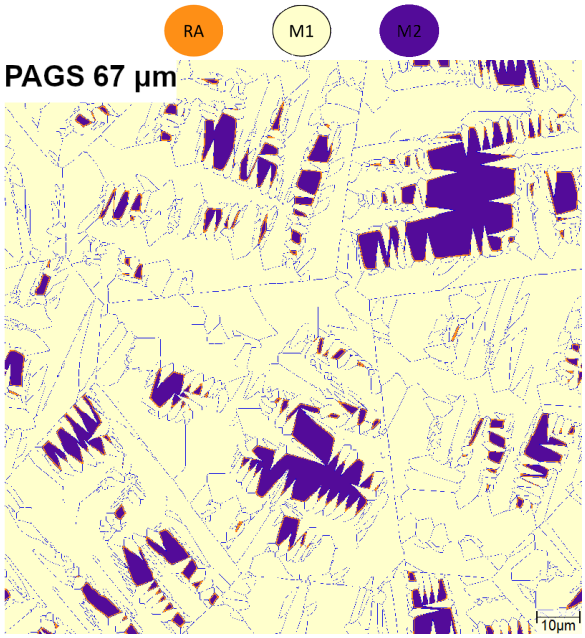

Figure 4.12: The final microstucture after partitioning for 50 s and quenching to room temperature for the case of PAGS of 67 μm

Chapter 5

Discussion

In this chapter, results are discussed in detail. Specifically, microstructures obtained by PFM are compared to those created experimentally to evaluate the model that was used. The effect of PAGS on the retained austenite and the way that carbon is redistributed during partitioning is also discussed. Then, the correlation of PAGS with the spatial distribution of austenite and how this affects the partitioning process is presented. Since the austenite grain size and carbon content of austenite being present in the final microstructure affect its mechanical stability, a prediction of this behaviour is proposed with respect to the PAGS.

5.1 Comparison of simulation results with experimental data

In figure 5.1 (a-f), the simulation microstructures are compared to the experimental images derived by the electron backscatter diffraction (EBSD) technique in the work of Celada-Casero et al. [12], the observations of this comparison are listed below.

- Martensite was simulated considering finite grains growing following specific orientations. In both the simulation and experimental microstructures (figure 5.1 a-c and d-e respectively), the martensite grains show a transition from an equiaxed to a columnar shape with increasing PAGS. For both cases, this occurs because the directional growth of martensite continues until an obstacle such as grain boundaries or another acicular grain hinders the growth. With increasing PAGS, there is more space for the nuclei to grow freely, resulting in elongated grains with an aspect ratio that is less than 1 as it has also been shown experimentally [32].

- The austenitic grains of both experimental and simulation microstructures are mainly in the form of block austenite for small PAGS but they form also film austenite with increasing PAGS. The film austenite that was detected by the EBSD and simulated by the PFM had a thickness in the order of a few hundreds of nm. Thinner austenite films (thickness of 20-100nm [51, 52]) were not visible by EBSD and were not simulated.

- With increasing PAGS, less and coarser austenite grains were present in both experimental and simulation microstructures.
- Significant grain size variation of ferrite in both experimental and simulation microstructures irrespective of the PAGS.
- The simulation failed to represent very small austenitic grains that were found to be present according to the EBSD data. For instance, grains of the size of those in the red circle in figure 5.1 (d) are not present in the simulation microstructures.
- Less and coarser austenitic grains are present in the simulations compared to the real microstructures of the same PAGS. This is presented in figure 5.8 where the average austenite grain size after the first quenching for the three different PAGSs is compared with the corresponding experimental values [12]. However, in both experimental and simulation microstructures the rate that austenite grain size increases with increasing PAGS declines. After a point, a further increase of PAGS does not reflect on the grain size of austenite on the final microstructure.

There are three main reasons for the discrepancies between the average austenite grain size after quenching of the experiments and the simulations.

- During the quenching simulation, the austenite grain size is controlled indirectly by controlling the way that martensite grows inside the austenitic matrix. The simulation of the displacive martensitic transformation as a diffusive transformation makes the control of the simulation microstructures challenging and matching the simulation austenite grain size with the experimentally measured values becomes difficult.
- A significantly higher resolution of the simulation (smaller grid spacing) would be needed to be used for the simulations to represent also very small austenite grains. This would decrease the mean grain size value of the domain, but it would dramatically increase the calculation time.
- Very thin film austenite (thinner than 100 nm) that is present in the experimental microstructures was ignored as a consequence of the low simulation resolution. So, the whole amount of austenite was simulated as block austenite, and consequently, larger blocks of austenite were used to achieve the desired austenite phase fraction in the simulations accounting also for the absence of thin-film austenite.

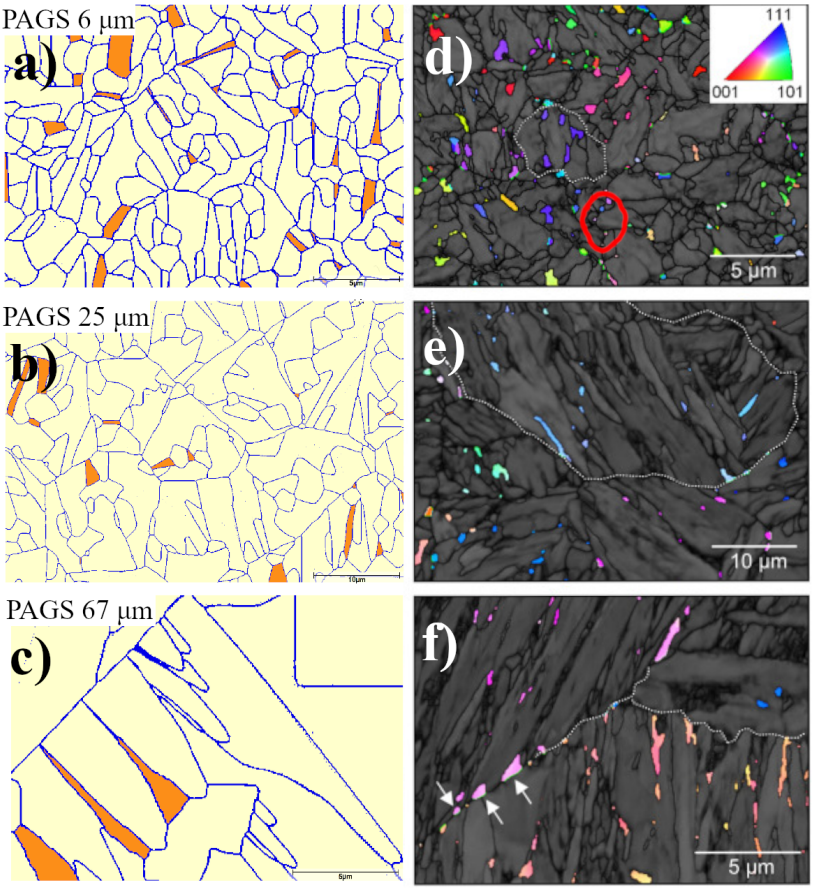

Figure 5.1: Comparison between the experimental and the simulation microstructures for the cases of PAGS of 6, 25 and 67 μm [12].

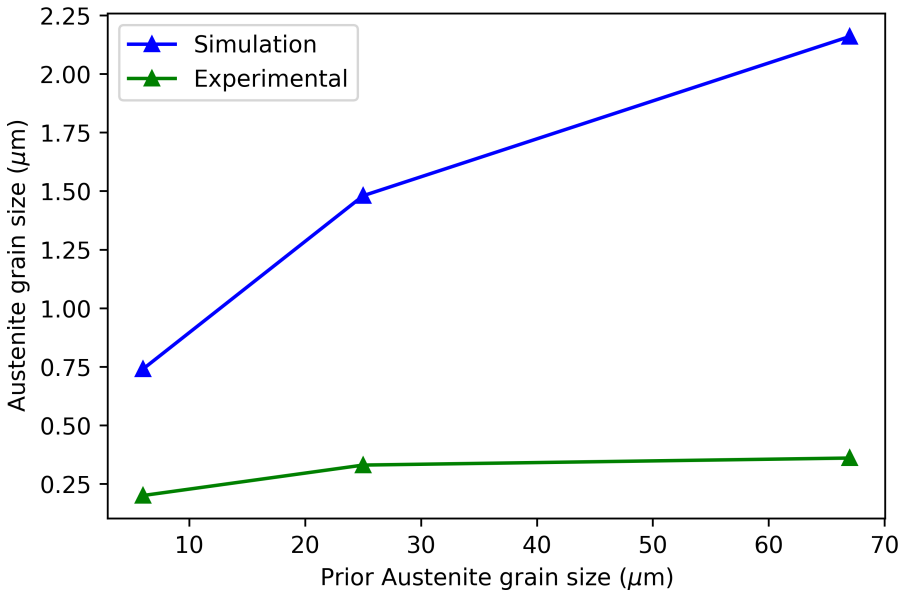

Figure 5.2: Comparison between the experimental and the simulation average austenite grain size after the first quenching for the cases of PAGS of 6 and 25 μm [12].

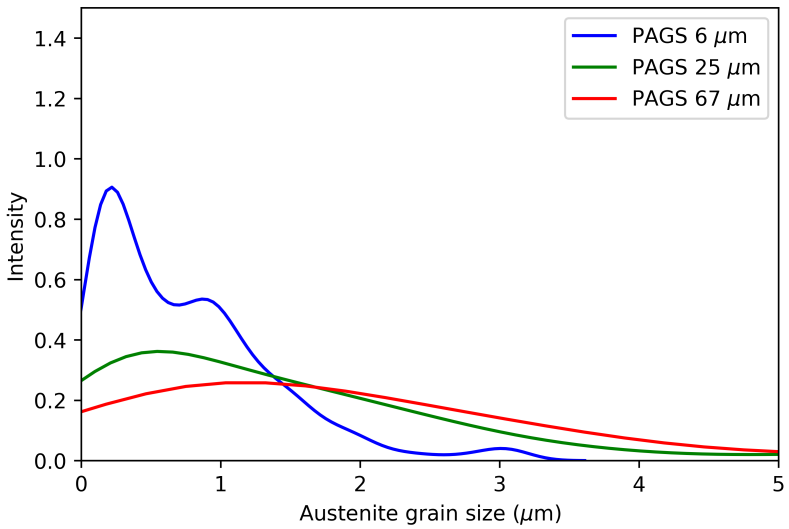

Figure 5.3: The grain size statistical distribution of austenite resulted from the first quenching for the three cases of PAGS of 6, 25, 67 μm

5.2 Effect of PAGS on carbon distribution

In figure 5.3 the grain size distributions of the austenitic grains that are present on the three microstructures right after the first quenching are compared. The grain size distributions become wider and their mean value increases with increasing PAGS. The width of the distribution affects the partitioning process. Specifically, In figure 5.4, for each of the microstructures of PAGS of 6 and 25 μm, the evolution of carbon content in the bulk of four different grains with respect to the partitioning time is depicted for partitioning time up to 4000 s. The carbon concentration measurements were taken from the core of the grains that is the center of mass of the 2-D shape.

According to figure 5.4, irrespective of the PAGS, the smaller grains of each microstructure of different PAGS are found to be enriched in carbon for short partitioning times. The carbon concentrations of those small grains are significantly higher than the one predicted by the CCE conditions. At the same time, the larger grains get enriched in carbon slowly until they reach the equilibrium value. Grains of intermediate size show a mixed behaviour between the two extremes. Note that a grain is considered large or small always by being compared to the rest grains of the microstructure that it belongs. This is confirmed by observing that grains of a specific size that behave as large grains for the case of PAGS of 6 μm behave as small grains in the microstructure of 67 μm despite the fact that the grain size is approximately the same in both cases (cases of 1.12 and 1.14 μm in figure 5.4). So, this behaviour is a phenomenon related to the grain size distribution and not the grain size of an individual grain. The variation in the carbon contents among the grains of the final

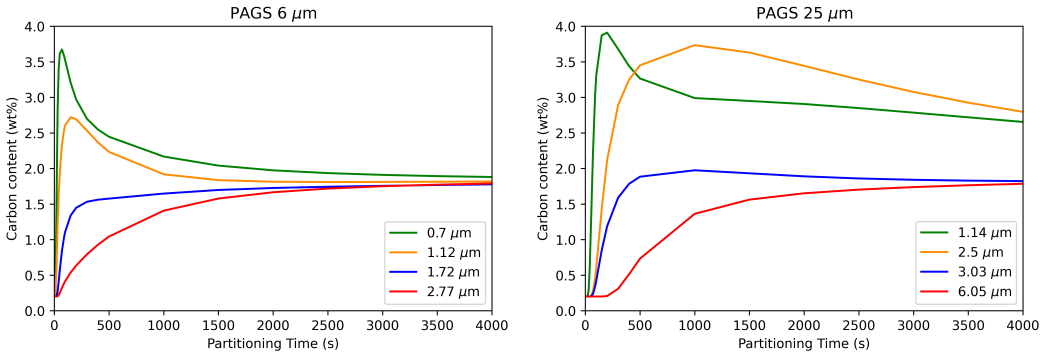

Figure 5.4: Evolution of carbon content in the core of austenitic grains with time for grains from microstructures of PAGS of 6 and 25μm; there is a strong relationship between the way that carbon enriches the grains and the grain size of examined grain relatively to the microstructure

microstructure has to be stronger for increasing PAGS because of the wider statistical austenite grain size distributions (figure 5.3).

In figure 5.4 and for the case of a grain of size of 1.14 μm, despite the large carbon content that is observed for short partitioning times, the excess carbon will diffuse out of the grain faster than the other grains of the same figure. This is probably explained by the relatively small grain size and the shorter distance that carbon has to diffuse on that specific grain. This trend was observed in most of the grains investigated, although the neighbourhood of the grain that is examined is crucial as it is discussed in the next section.

The austenite grain size distributions after the first quenching become wider with increasing PAGS. So, differences in the carbon content between grains of the same microstructure become more important with increasing PAGS, this can have three important effects for a real microstructure.

- It can affect the way that carbon partitions in austenite because carbon may partition inside small grains instead of enriching the larger ones.
- It can give rise to carbide precipitation because of the locally high carbon concentrations that are achieved especially to small grains
- It can affect the mechanical stability of the grains and consequently, the trip effect.

A way to visualise how carbon is distributed in austenite during partitioning is by plotting the fraction of austenite that is sufficiently enriched in carbon to be stable at room temperature with respect to the average carbon concentration of the whole austenite of the microstructure (figure 5.5). So, for the same average carbon

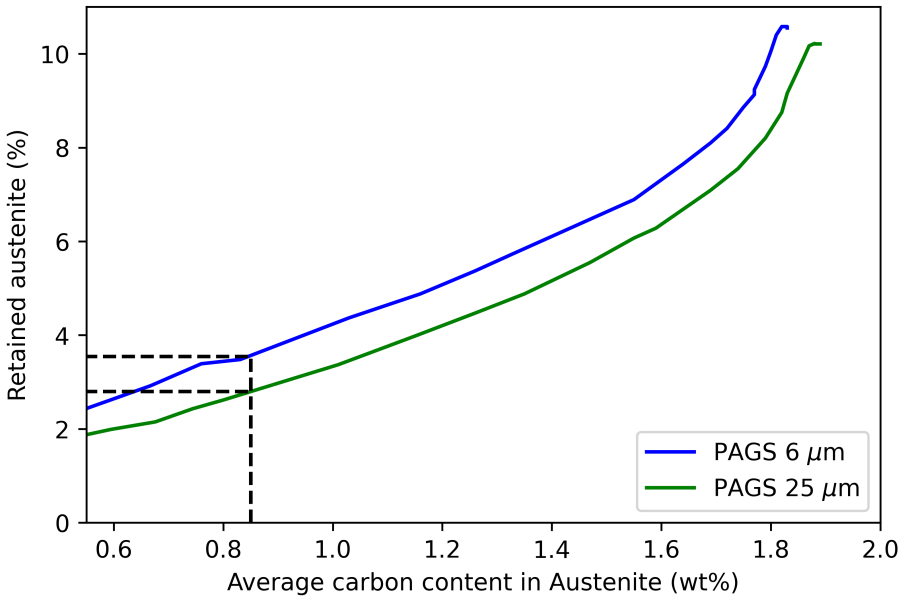

Figure 5.5: The fraction of austenite that is sufficiently enriched in carbon to be thermally stable at room temperature versus the average carbon content in austenite for microstructures of PAGS of 6 and 25μm.

concentration in austenite, the fraction of austenite that is sufficiently enriched in carbon is an index of how effectively carbon is distributed in the phase.

Figure 5.5 shows that the microstructure with PAGS of 6 μm had a higher fraction of sufficiently enriched austenite than the PAGS of 25 μm for the same average carbon content in austenite. This means that in the microstructure with the large PAGS, carbon is less uniformly distributed, with areas with significantly higher carbon content and areas that are depleted in carbon both being present. Those areas are mainly of two kinds: (a) Small grains that tend to retain significantly larger amounts of carbon than the equilibrium value. (b) The outer area of the austenitic grains where carbon did not have enough time to diffuse towards the bulk of the grain. It was also observed for both cases that from a very early stage, the average carbon content is above the critical value that is 0.85% wt. At this point, about 2.6% and 3.5% of the austenite is sufficiently enriched in carbon for PAGS of 6 and 25 μm respectively.

An example of these two areas is shown in figure 5.6. Grain A and B are taken from the simulation of PAGS of 6 μm where partitioning took place for 40 s. In grain A, we see that in most of its area the carbon content is less than 1% wt. that means that the local carbon concentration is close to the critical value for thermal stabilisation that is 0.85 % wt. In contrast, in grain B and for equal partitioning time, the local carbon content is above 2.7% that is significantly larger than the critical value. Furthermore, the outer region of grain A shows also a higher carbon concentration. The above means that carbon is not distributed effectively because there are austenitic areas

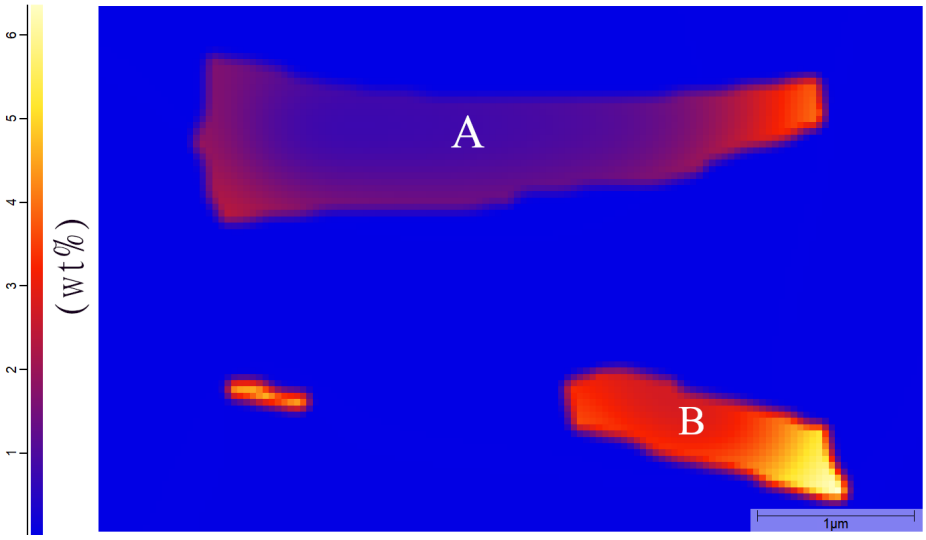

Figure 5.6: Carbon distribution of two grains of different size from the partitioning simulations of the microstructure of PAGS of 6 μm.

with excess carbon content and areas with local carbon content close to the critical value.

A microstructure with large PAGS (and consequently large austenitic grains during partitioning) has smaller fcc/bcc interface total surface compared to a microstructure with small PAGS. This means that for a fixed phase fraction, large PAGS involves less interface and more carbon has to diffuse through a smaller interface area. In combination with the low diffusivity of carbon in the fcc phase, the carbon concentration in the outer region of the grains is increased especially at the beginning of the partitioning process.

Similarly, the smaller grains of a microstructure achieve high carbon concentrations on their outer region for short partitioning times. At a later stage, the carbon concentrated at the outer region of the grains diffuse towards the core of the grain. If the grain is too small to accommodate all the amount of carbon its concentration increases, usually above the equilibrium value, and for longer partitioning times, the reversion of the diffusion direction takes place. Carbon will diffuse back to martensite and then to larger austenitic grains with lower carbon concentrations. The different carbon concentrations among the austenitic grains give rise to diffusion from the richer grains to the ones with low carbon concentration through martensite to achieve a further decrease of the Gibbs free energy. That is the reason why the diffusion direction is reversed. This goes on until austenite has the equilibrium carbon content in its whole extent.

For small PAGS, austenite showed a fine distribution in the microstructure compared to large PAGS. This happens because, for small PAGS, the blocks of austenite

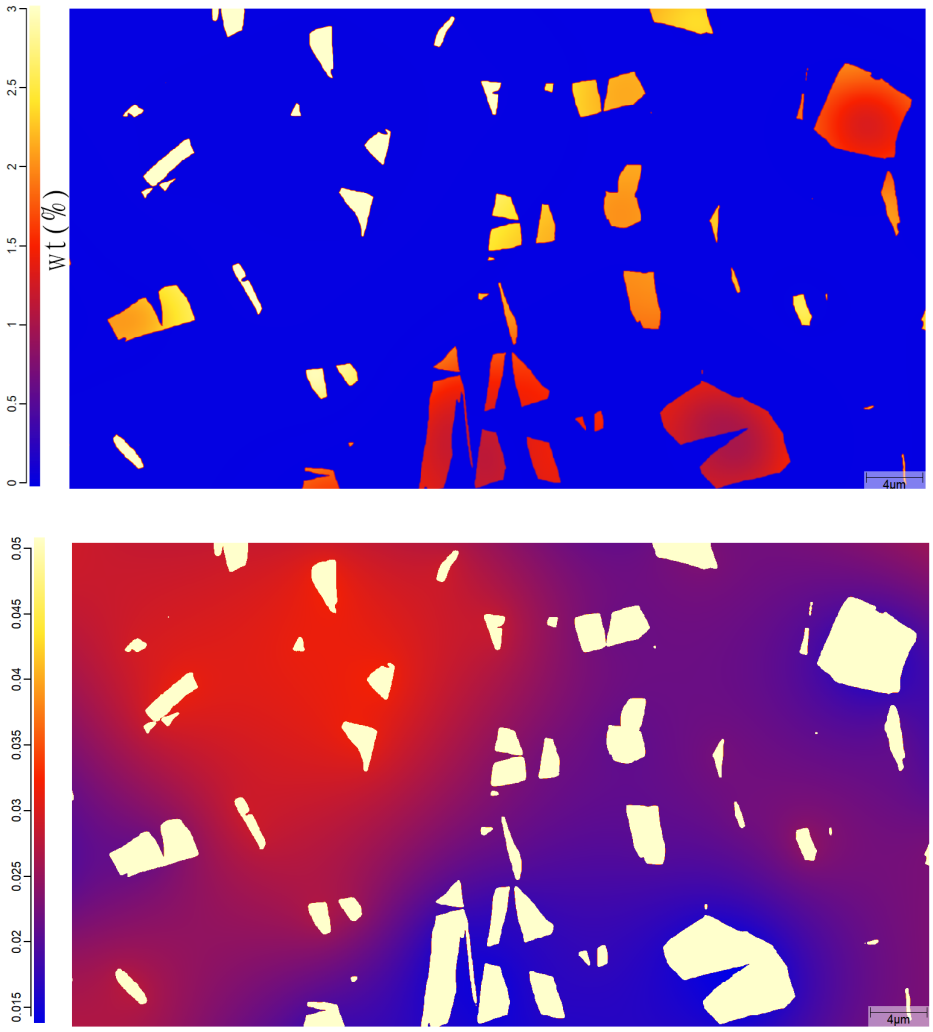

Figure 5.7: An area of the microstructure of PAGS of 25 μm that shows that the austenite that belongs to neighbourhoods with high austenite density is depleted in carbon and diffusion from long distance has to take place to enrich the densely distributed austenite.

that are shaped after the first quenching originate from a high number of parent austenite grains resulting in finer grains that are sporadically distributed.

In figure 5.7 the carbon distribution of a microstructure of PAGS of 25 μm after partitioning for 1000 s is presented. It can be observed that the sparsely distributed grains exhibit higher carbon content. In figure 5.7 the carbon distribution of martensite is also visible. Martensite on the area that contains the sparsely distributed austenite grains is rich in carbon. This means that the excess carbon that is in those austenitic grains and the surrounding martensite will diffuse to the depleted area.

A simple way to quantify how sparse is the spatial distribution of austenite during partitioning is presented here, and it is based on the work of Kin Ming Kam et al. for particle distributions [53]. The idea is to separate the microstructure in quadrats and then to estimate the phase fraction of austenite for each quadrat. Then the index

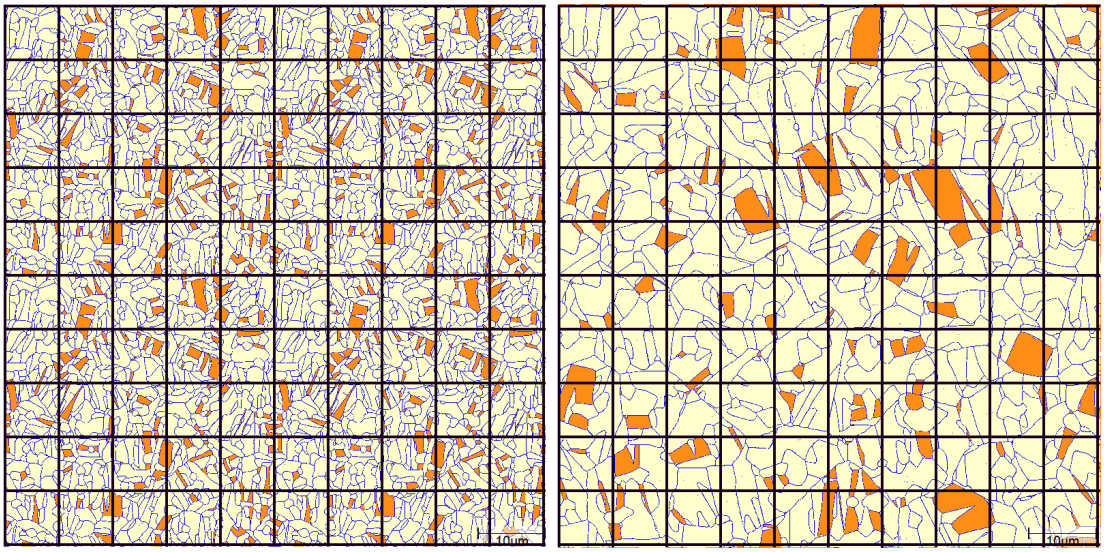

Figure 5.8: The grids that were created to quantify how sparsely austenite is distributed in the microstructures that undergo partitioning.

of dispersion (ID) that is given in equation 5.4.1 is calculated where q is the number of quadrats, $\bar{x}$ and s are the mean value and standard deviation of austenite phase fraction of the quadrats. The higher the ID value, the more clustered the austenite is. The ID index was estimated for the cases of PAGS of 6 and 25 μm. The domains that were selected for the two cases had dimensions of 80×80 μm and they were separated in 100 quadrants. The ID was 53.64 and 146.52 for the PAGS of 6 and 25 μm respectively, indicating a more even spatial distribution of austenite for the case of 6 μm that means that fewer clusters such as in the 5.8 are present in the microstructure and so, partitioning efficiency is enhanced.

$$ID = \frac{(q-1)s^2}{\bar{x}} \tag{5.2.1}$$

5.3 Effect of PAGS on the retained austenite

In figure 5.9 the fraction of austenite that is retained for different partitioning times is presented for the three microstructures of different PAGS that were examined. The phase fraction of austenite before partitioning was approximately 0.105 for all the PAGSs. The critical carbon value for thermal stabilisation was 0.85% wt. as it was proposed in the previous chapter.

It can be seen that the PAGS affects significantly the partitioning time required for stabilisation of the whole amount of austenite. The time that is needed for stabilisation decreases with decreasing PAGS, which is in agreement with the literature findings [32]. Specifically, for the case of PAGS of 6 μm almost all the austenite is

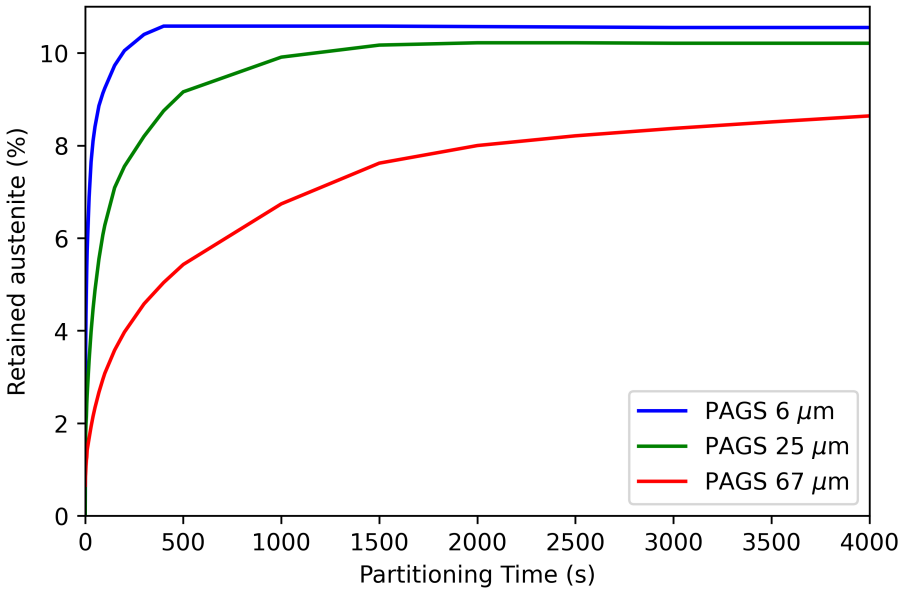

Figure 5.9: Comparison of the fraction of austenite that is retained with respect to the partitioning time for PAGS of 6,25 and 67 μm; smaller PAGS result in faster partitioning

retained after partitioning for approximately 200 s while for the case of PAGS of 25 μm about 1000 s required. The microstructure with PAGS of 67 μm did not achieve to retain the whole amount of austenite even after 4000 s of partitioning.

However, Celada-Casero et al. [12] showed experimentally that 50 s of partitioning was enough to minimise the effect of PAGS in the final phase fractions for a PAGS up to 67μm. Therefore, the partitioning time required to retain the whole amount of austenite that is available was overestimated for all the microstructures in the simulations when compared to experimental observations.

The main reason for the large difference is that the quenching simulations overestimate the grain size of austenite that finally undergoes partitioning. The larger austenitic grains of the simulations require more time to be enriched in carbon than the grains of the experimental microstructures due to the large distance that carbon has to diffuse through. Moreover, the more even spatial distribution of austenite during partitioning in experimental microstructures increases the α'/γ interface retarding the partitioning of carbon.

Nevertheless, the austenite grain size distributions after the first quenching that were derived from the simulations are similar to other research works [54, 55] and the results contribute to the better understanding of the carbon kinetics during the partitioning process.

Considering the film austenite with thickness below 100 nm that was not taken into account in the simulations, it is known that it is enriched in carbon significantly faster

than the block austenite due to the short distance that carbon has to diffuse [12].

5.4 Limitations of the simulations

- An important limitation of the simulations was the inability to represent thin-film austenite with widths lower than 100 nm for the reasons explained.

- Bainite transformation was not considered in this study. In the study of Celada-Casero et al. [12] small fractions of bainite were found even for the short partitioning time of 50 s, so it is expected that more bainite will be present at longer partitioning times such as the ones of the present work.

- Carbide precipitation was ignored in this study. Nevertheless, during the simulations, high carbon concentrations were observed at the interface between the fcc and bcc phases and especially, at the smallest grains of each microstructure. The concentration values where sometimes even higher than the eutectoid composition, which means that cementite could probably precipitate at these sites, this was also observed in other studies [17].

- A 2-D model was used, so diffusion is restricted only at two directions instead of three.

5.5 Assesment of mechanical stability

Literature showed that both the size and the carbon content affect the mechanical stability of austenite and consequently, the TRIP effect [54, 56]. Specifically, large austenitic grains with a locally low carbon content tend to transform easier under mechanical strain and vice versa. The PAGS affect both the size and the carbon distribution of the austenite that is present in the final microstructure so it should also affect the TRIP phenomenon.

To investigate how the PAGS can affect the mechanical stability and the TRIP phenomenon, the carbon content along with the grain size of about 100 austenitic grains were measured from the simulated microstructures of PAGS of 6 and 25 μm. Furthermore, the minimum partitioning time that results in a microstructure free of fresh martensite was selected for each case of PAGS. The resulted points were separated into 14 clusters of points, for easier interpretation, plotted in figure 5.10. Then, the graph in figure 5.10 was separated into three zones to explain how the combination of austenite grain size and carbon content can affect the TRIP effect.

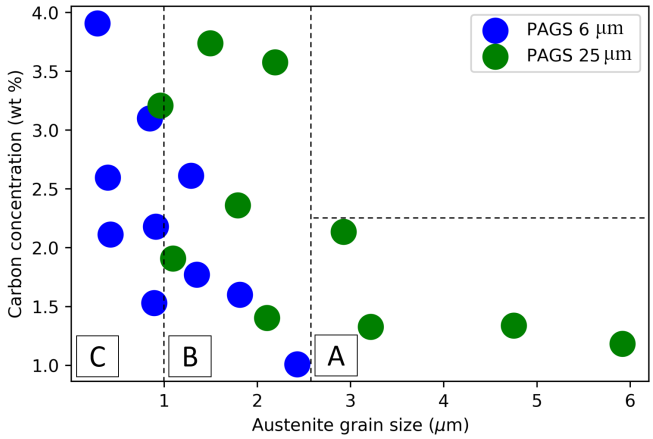

Figure 5.10: The carbon content and the size of about 100 grains was measured from the simulations of PAGS of 6 and 25μm. The differences in size and carbon content have an impact on the TRIP effect with the large and carbon depleted grains being less stable under strain conditions.

- Zone A: For the case of PAGS of 25 μm some large austenite grains are present with relatively low carbon content. These grains are expected to transform to martensite at low strains so, the TRIP effect is expected to take place earlier than in the microstructure of PAGS of 6μm.
- Zone B: The microstructure of PAGS of 25 μm tends to have grains with higher concentrations in carbon compared to the ones of the microstructure of PAGS of 6 μm. This means that the grains of PAGS of 25 μm are more stable and they will require higher strain to transform to martensite compared to ones of PAGS of 6 μm that belong in the same zone.
- Zone C: There are a lot of small grains of this size present in the microstructure of PAGS of 6 μm that are enriched in carbon and they are expected to be mechanically stable at relatively high strains.

So, based on this idea, the mechanical stability will be lower at low strains for the microstructure of PAGS of 25 μm then, at intermediate strains, the microstructure of PAGS of 6 μm will exhibit lower mechanical stability and at high strains, most of the austenite is expected to have been transformed for the microstructure of PAGS of 25 μm while for the microstructure of PAGS of 6 μm plenty of small austenitic grains that are highly enriched in carbon will still be present.

Considering the film austenite that was not modelled (thickness less than 100 nm), despite the fact that usually exhibits lower local carbon concentration compared to block austenite, because of its shape it shows high mechanical stability and it is expected to transform for strains that are close to the necking point [54].

Chapter 6

Conclusions/Future work

6.1 Conclusions

The effect of prior austenite grain size on the quenching and partitioning process was studied using phase-field modelling simulations. Three different PAGSs were selected, 6, 25 and 67 μm. MICRESS© software was employed to create the three initial fully austenitic microstructures and to perform the simulations. At the simulation of the first quenching, equal fractions of martensite were introduced in all the microstructures. The partitioning step was simulated for different durations up to 4000 s at 400 $^{\circ}C$. Based on the carbon distribution maps produced by the software at the end of partitioning, a criterion was used to decide if austenite was sufficiently enriched in carbon on a local level to get stable at room temperature. The final microstructures were simulated and the main conclusions from the discussion of the results are listed below.

- The martensitic grains of the quenching simulations showed a transition from an equiaxed shape to a columnar shape with increasing PAGS. Austenite was found to be in the shape of block austenite for all the PAGS that were examined while thick film austenite with thickness in the order of hundreds of nm was also present with increasing PAGS. The mean austenite grain size right after the first quenching increases with increasing PAGS but with a decreasing rate. The above observations agree with the experimental data.

- Real Q&P microstructures also consist of a considerable fraction of film austenite with thickness less than 100 nm that was not simulated due to simulation resolution restrictions. The inability to produce a microstructure consisting of thin-film (less than 100 nm) austenite led to the representation of the whole amount of austenite as block austenite. This, along with the indirect control of the austenite grain morphology during the martensitic transformation, led to the overestimation of the mean austenite grain size right after the first quenching.

- For short partitioning times, the microstructure of PAGS of 6 μm managed to retain higher fractions of austenite than the microstructure of PAGS of 25

μm. Both microstructures retained all their austenite after 200 and 1000 s, respectively. The microstructure of PAGS of 67 μm retained significantly less austenite for short partitioning times compared to the other two cases and did not achieve to retain all its austenite after partitioning for 4000 s. This shows that partitioning efficiency has to be strongly connected to the PAGS.

- The spatial distribution of austenite is also of great importance during partitioning. It was found that microstructures with small PAGS showed an even spatial distribution of austenite. This makes partitioning more efficient because austenite is mixed better with martensite making partitioning of carbon easier since carbon does not have to diffuse through large distances in martensite before partitioning to austenite.

- Microstructures with small PAGS show higher partitioning efficiency because of the shorter distance that carbon had to diffuse in the fcc phase. Moreover, the smaller austenite grains imply a larger γ/α' total interface area and partitioning of carbon takes place faster.

- The width of the austenite grain size distribution right before partitioning plays an important role in the Q&P process. Moreover, it becomes wider with increasing PAGS. The smaller austenitic grains of a distribution (irrespective of the PAGS) were found to have a significantly higher carbon content compared to the large grains of the same microstructure, especially for short partitioning times. For small PAGS with narrow grain size distributions, smaller differences in the carbon content among the grains were observed. This phenomenon can affect partitioning efficiency since carbon partitions into the smaller grains that have excess carbon content instead of enriching the larger ones (something that will happen later).

- The high carbon concentrations that were observed locally, especially on the smaller austenitic grains of each microstructure can give rise to carbide precipitation. However, the nature of the simulation does not allow safe conclusions about the sites where nucleation is most likely.

- The variation in austenite grain size and carbon content resulting at the end of the Q&P process which becomes more severe for large PAGS can also affect the mechanical stability of austenite. The wider the austenite grain size distribution after quenching, the larger the variation among the local carbon contents of the RA. A comparison between the cases of PAGS of 6 and 25 μm showed that the microstructure of PAGS of 6 μm should show higher mechanical stability for

low and high strains while the microstructure of PAGS of 25 μm will be more stable for intermediate strains.

6.2 Future work

- The simulation model that is proposed on this study for the simulation of the Q&P process does not consider thin-film austenite (thickness less than 100 nm) that is retained between laths, blocks and other subunits of martensite. Moreover, the grain size of austenite that is still present after the first quenching is larger than the experimental values. The use of a higher resolution that is able to describe grains and films of a lower scale, along with the optimisation of the simulation conditions of the martensitic transformation, can give a better description that matches better the experimental results.

- The critical carbon content for the thermal stabilisation of austenite at room temperature that was used for the simulations of the final quenching was 0.85 % wt. However, this value has to be strongly connected to the grain size and the way that the transformations stresses are accommodated by the austenitic grains of the microstructure, but both factors were ignored on the present study. Small grains under high stresses will probably require less carbon to be thermally stable at room temperature. The dependence of the critical carbon content for thermal stabilisation on the PAGS can be studied by combining experimental results and simulations of the stresses by using the elastic module of MICRESS©.

Bibliography

[1] John G. Speer, Fernando C. Rizzo Assunção, David K. Matlock, and David V. Edmonds. The "quenching and partitioning" process: Background and recent progress. *Materials Research*, 8(4):417–423, 2005.

[2] Reza Tolouei and Helena Titheridge. Vehicle mass as a determinant of fuel consumption and secondary safety performance. *Transportation Research Part D: Transport and Environment*, 14(6):385–399, 2009.

[3] Tarun Nanda, Vishal Singh, Virender Singh, Arnab Chakraborty, and Sandeep Sharma. Third generation of advanced high-strength steels: Processing routes and properties. *Proceedings of the Institution of Mechanical Engineers, Part L: Journal of Materials: Design and Applications*, 233(2):209–238, 2019.

[4] Jingwei Zhao and Zhengyi Jiang. Thermomechanical processing of advanced high strength steels. *Progress in Materials Science*, 94:174–242, 2018.

[5] A. K. Chandan, G. K. Bansal, J. Kundu, J. Chakraborty, and S. Ghosh Chowdhury. Effect of prior austenite grain size on the evolution of microstructure and mechanical properties of an intercritically annealed medium manganese steel. *Materials Science and Engineering A*, 2019.

[6] Javier Hidalgo and Maria Jesus Santofimia. Effect of Prior Austenite Grain Size Refinement by Thermal Cycling on the Microstructural Features of As-Quenched Lath Martensite. *Metallurgical and Materials Transactions A: Physical Metallurgy and Materials Science*, 47(11):5288–5301, 2016.

[7] S Morito, H Saito, T Ogawa, T Furuhara, and T Maki. Effect of austenite grain size on the morphology and crystallography of lath martensite in low carbon steels. *ISIJ international*, 45(1):91–94, 2005.

[8] S. Morito, H. Tanaka, R. Konishi, T. Furuhara, and T. Maki. The morphology and crystallography of lath martensite in Fe-C alloys. *Acta Materialia*, 2003.

[9] S. Morito, X. Huang, T. Furuhara, T. Maki, and N. Hansen. The morphology and crystallography of lath martensite in alloy steels. *Acta Materialia*, 2006.

[10] Jun Zhang, Hua Ding, R. D.K. Misra, and Chao Wang. Enhanced stability of retained austenite and consequent work hardening rate through pre-quenching

prior to quenching and partitioning in a Q-P microalloyed steel. *Materials Science and Engineering A*, 611:252–256, 2014.

[11] Mahdi Karam-Abian, Abbas Zarei-Hanzaki, Hamidreza Abedi, Sepideh Ghodrat, Farideh Hajy-Akbary, and Leo Kestens. The Effect of Martensite-Austenite Constituent Characteristics on the Mechanical Behavior of Quenched-Partitioned Steel at Room Temperature. *Steel Research International*, 90(3), 2019.

[12] Carola Celada-Casero, Cees Kwakernaak, Jilt Sietsma, and Maria Jesus Santofimia. The influence of the austenite grain size on the microstructural development during quenching and partitioning processing of a low-carbon steel. *Materials and Design*, 178, 2019.

[13] M. J. Santofimia, L. Zhao, R. Petrov, C. Kwakernaak, W. G. Sloof, and J. Sietsma. Microstructural development during the quenching and partitioning process in a newly designed low-carbon steel. *Acta Materialia*, 59(15):6059–6068, 2011.

[14] Jorge Otubo, Fabiana C. Nascimento, Paulo R. Mei, Lisandro P. Cardoso, and Michael J. Kaufman. Influence of austenite grain size on mechanical properties of stainless SMA. *Materials Transactions*, 43(5):916–919, 2002.

[15] Feng Huang, Jilan Yang, Zhenghong Guo, Shipu Chen, Yonghua Rong, and Nailu Chen. Effect of Partitioning Treatment on the Mechanical Property of Fe-0.19C-1.47Mn-1.50Si Steel with Refined Martensitic Microstructure. *Metallurgical and Materials Transactions A: Physical Metallurgy and Materials Science*, 47(3):1072–1082, 2016.

[16] M. G. Mecozzi, J. Eiken, M. J. Santofimia, and J. Sietsma. Phase field modelling of microstructural evolution during the quenching and partitioning treatment in low-alloy steels. *Computational Materials Science*, 112:245–256, 2016.

[17] Y. Takahama, M. J. Santofimia, M. G. Mecozzi, L. Zhao, and J. Sietsma. Phase field simulation of the carbon redistribution during the quenching and partitioning process in a low-carbon steel. *Acta Materialia*, 2012.

[18] Hemantha Kumar Yeddu. Phase-field modeling of austenite grain size effect on martensitic transformation in stainless steels. *Computational Materials Science*, 2018.

[19] Matthias Militzer. Phase field modeling of microstructure evolution in steels. *Current Opinion in Solid State and Materials Science*, 15(3):106–115, 2011.

[20] Jilt Sietsma. Physical modelling the microstructure formation in advanced high-strength steels. In *Materials Science Forum*, volume 762, pages 194–209. Trans Tech Publ, 2013.

[21] D. P. Koistinen and R. E. Marburger. A general equation prescribing the extent of the austenite-martensite transformation in pure iron-carbon alloys and plain carbon steels, 1959.

[22] S. M.C. van Bohemen and J. Sietsma. Martensite formation in partially and fully austenitic plain carbon steels. *Metallurgical and Materials Transactions A: Physical Metallurgy and Materials Science*, 40(5):1059–1068, 2009.

[23] M. J. Santofimia, J. G. Speer, A. J. Clarke, L. Zhao, and J. Sietsma. Influence of interface mobility on the evolution of austenite-martensite grain assemblies during annealing. *Acta Materialia*, 2009.

[24] J. Speer, D. K. Matlock, B. C. De Cooman, and J. G. Schroth. Carbon partitioning into austenite after martensite transformation. *Acta Materialia*, 2003.

[25] Joseph A. Lobo and Gordon H. Geiger. Thermodynamics of carbon in austenite and Fe-Mo austenite. *Metallurgical Transactions A*, 7(8):1359–1364, 1976.

[26] Joseph A. Lobo and Gordon H. Geiger. Thermodynamics and solubility of carbon in ferrite and ferritic Fe-Mo alloys. *Metallurgical Transactions A*, 7(8):1347–1357, 1976.

[27] M. J. Santofimia, L. Zhao, and J. Sietsma. Model for the interaction between interface migration and carbon diffusion during annealing of martensite-austenite microstructures in steels. *Scripta Materialia*, 2008.

[28] John Crank. *The mathematics of diffusion*. Oxford university press, 1979.

[29] Harry Bhadeshia and Robert Honeycombe. *Steels: microstructure and properties*. Butterworth-Heinemann, 2017.

[30] JG Speer, AM Streicher, DK Matlock, F Rizzo, and G Krauss. Quenching and partitioning: a fundamentally new process to create high strength trip sheet microstructures. In *Symposium on the Thermodynamics, Kinetics, Characterization and Modeling of: Austenite Formation and Decomposition*, pages 505–522, 2003.

[31] E. Jimenez-Melero, N. H. van Dijk, L. Zhao, J. Sietsma, S. E. Offerman, J. P. Wright, and S. van der Zwaag. Characterization of individual retained austenite grains and their stability in low-alloyed TRIP steels. *Acta Materialia*, 2007.

[32] Carola Celada-Casero, Jilt Sietsma, and Maria Jesus Santofimia. The role of the austenite grain size in the martensitic transformation in low carbon steels. *Materials and Design*, 2019.

[33] GB Olson and Morris Cohen. Kinetics of strain-induced martensitic nucleation. *Metallurgical transactions A*, 6(4):791, 1975.

[34] Yoshikazu Matsuoka, Tatsuya Iwasaki, Nobuo Nakada, Toshihiro Tsuchiyama, and Setsuo Takaki. Effect of grain size on thermal and mechanical stability of austenite in metastable austenitic stainless steel. *ISIJ International*, 53(7):1224–1230, 2013.

[35] H. K.D.H. Bhadeshia and D. V. Edmonds. Bainite in silicon steels: New composition-property approach. *Metal Science*, 17(9):420–425, 1983.

[36] Lawrence Cho, Eun Jung Seo, and Bruno C. De Cooman. Near-Ac3 austenitized ultra-fine-grained quenching and partitioning (Q&P) steel. *Scripta Materialia*, 2016.

[37] Jeongho Han, Seung Joon Lee, Chan Young Lee, Sukjin Lee, Seo Yeon Jo, and Young Kook Lee. The size effect of initial martensite constituents on the microstructure and tensile properties of intercritically annealed Fe-9Mn-0.05C steel. *Materials Science and Engineering A*, 633:9–16, 2015.

[38] EI Galindo-Nava and PEJ Rivera-Díaz-del Castillo. A model for the microstructure behaviour and strength evolution in lath martensite. *Acta Materialia*, 98:81–93, 2015.

[39] Setsuo Takaki, Kazuhiro Fukunaga, Junaidi Syarif, and Toshihiro Tsuchiyama. Effect of grain refinement on thermal stability of metastable austenitic steel. *Materials Transactions*, 45(7):2245–2251, 2004.

[40] Bin Chen, Juhua Liang, Tao Kang, Ronghua Cao, Cheng Li, Jiangtao Liang, Feng Li, Zhengzhi Zhao, and Di Tang. A study of the optimum quenching temperature of steels with various hot rolling microstructures after cold rolling, quenching and partitioning treatment. *Metals*, 8(8), 2018.

[41] Z. R. Hou, X. M. Zhao, W. Zhang, H. L. Liu, and H. L. Yi. A medium manganese steel designed for water quenching and partitioning. *Materials Science and Technology (United Kingdom)*, 34(10):1168–1175, 2018.

[42] Eun Jung Seo, Lawrence Cho, and Bruno C. De Cooman. Kinetics of the partitioning of carbon and substitutional alloying elements during quenching and partitioning (Q&P) processing of medium Mn steel. *Acta Materialia*, 2016.

[43] Ji Hoon Kim, Sea Woong Lee, Kyooyoung Lee, Jin Kyung Kim, and Dong Woo Suh. Effect of Prior Austenite Grain Size on Hole Expansion Ratio of Quenching and Partitioning Processed Medium-Mn Steel. *Jom*, 71(4):1366–1374, 2019.

[44] Heiwen Luo, Lie Zhao, Suzelotte O. Kruijver, Jilt Sietsma, and Sybrand Van der Zwaag. Effect of Intercritical Deformation on Bainite Formation in Al-containing TRIP Steel. *ISIJ International*, 43(8):1219–1227, 2003.

[45] S. M.C. van Bohemen. Bainite growth retardation due to mechanical stabilisation of austenite. *Materialia*, 2019.

[46] M. J. Santofimia, L. Zhao, R. Petrov, and J. Sietsma. Characterization of the microstructure obtained by the quenching and partitioning process in a low-carbon steel. *Materials Characterization*, 2008.

[47] I. Steinbach, F. Pezzolla, B. Nestler, M. Seeßelberg, R. Prieler, G. J. Schmitz, and J. L.L. Rezende. A phase field concept for multiphase systems. *Physica D: Nonlinear Phenomena*, 1996.

[48] J. Eiken, B. Böttger, and I. Steinbach. Multiphase-field approach for multicomponent alloys with extrapolation scheme for numerical application. *Physical Review E - Statistical, Nonlinear, and Soft Matter Physics*, 73(6):1–9, 2006.

[49] www.micress.de.

[50] U. Grafe, B. Böttger, J. Tiaden, and S. G. Fries. Coupling of multicomponent thermodynamic databases to a phase field model: application to solidification and solid state transformations of superalloys. *Scripta Materialia*, 42(12):1179–1186, 2000.

[51] C. Y. Wang, J. Shi, W. Q. Cao, and H. Dong. Characterization of microstructure obtained by quenching and partitioning process in low alloy martensitic steel. *Materials Science and Engineering A*, 2010.

[52] Fei Peng, Yunbo Xu, Jiayu Li, Xingli Gu, and Xu . Interaction of martensite and bainite transformations and its dependence on quenching temperature in intercritical quenching and partitioning steels. *Materials and Design*, 2019.

[53] Kin Ming Kam, Li Zeng, Qiang Zhou, Richard Tran, and Jian Yang. On assessing spatial uniformity of particle distributions in quality control of manufacturing processes. *Journal of Manufacturing Systems*, 32(1):154, 2013.

[54] Dorien De Knijf, Cecilia Föjer, Leo A.I. Kestens, and Roumen Petrov. Factors influencing the austenite stability during tensile testing of Quenching and Partitioning steel determined via in-situ Electron Backscatter Diffraction. *Materials Science and Engineering A*, 638:219–227, 2015.

[55] E. Jimenez-Melero, N. H. van Dijk, L. Zhao, J. Sietsma, S. E. Offerman, J. P. Wright, and S. van der Zwaag. The effect of aluminium and phosphorus on the stability of individual austenite grains in TRIP steels. *Acta Materialia*, 57(2):533–543, 2009.

[56] R. Blondé, E. Jimenez-Melero, L. Zhao, J. P. Wright, E. Brück, S. Van Der Zwaag, and N. H. Van Dijk. High-energy X-ray diffraction study on the temperature-dependent mechanical stability of retained austenite in low-alloyed TRIP steels. *Acta Materialia*, 60(2):565–577, 2012.